Aalto University
School of Chemical
Engineering

Henri Sydänmaanlakka

mRNA detection using constrained DNA hybridization chain reaction on nanoparticles

Master´s Programme in Life Science Technologies
Major in Biosystems and Biomaterials Engineering

Master's thesis for the degree of Master of Science in Technology submitted for inspection, Espoo, 24 March, 2020.

Supervisor: Professor Mauri Kostiainen

Advisor: Ph.D. Qing Liu

Aalto University
School of Chemical
Engineering

Author Henri Sydänmaanlakka

Title of thesis mRNA detection using constrained DNA hybridization chain reaction on nanoparticles

Degree Programme Life Science Technologies

Major Biosystems and Biomaterials Engineering

Thesis supervisor Professor Mauri Kostiainen

Thesis advisor(s) / Thesis examiner(s) Ph.D. Qing Liu

Date 24.03.2020 **Number of pages** 48 **Language** English

Abstract

Hybridization chain reaction (HCR) is a powerful tool for the detection of RNA with excellent sensitivity. However, the speed and sensitivity of HCR is usually limited due to its reliance on diffusion kinetics. Constraining the chain reaction in close space allows faster detection speeds and higher sensitivity than non-constrained ones because no diffusion process is needed.

The aim of this thesis is to improve the RNA detection speed and sensitivity using HCR. To achieve this, two DNA HCR hairpin monomers were used. After confirming the successful HCR in solution, the HCR monomers were constrained on nanoparticles. The attachment of the DNA hairpins on the surface of the nanoparticles were studied via UV/Vis spectroscopy and verified with transmission electron microscopy. The HCR on top of nanoparticles was studied by measuring time-dependent fluorescence intensity.

Successful HCR in solution was verified with polyacrylamide gel electrophoresis and fluorescence measurement and successful attachment of hairpin DNA on top of both gold and silicon nanoparticles was demonstrated. However, the DNA hairpins were partially opened after attachment, which induced the HCR in the absence of the initiator strand. This was verified with polyacrylamide gel electrophoresis. Nevertheless, HCR was proven to be feasible on nanoparticles' surface and the design needs to be optimized before the method is viable for RNA detection *in vivo*.

Keywords Hybridization chain reaction, RNA detection, nanoparticles, spherical nucleic acids

Aalto-yliopisto
Kemian tekniikan korkeakoulu

Tekijä Henri Sydänmaanlakka

Työn nimi mRNA detektointi käyttämällä DNA hybridisaatioketjureaktiota nanopartikkelien pinnalla

Koulutusohjelma Life Science Technologies

Pääaine Biosystems and Biomaterials Engineering

Työn valvoja Professori Mauri Kostiainen

Työn ohjaaja(t)/Työn tarkastaja(t) FT Qing Liu

Päivämäärä 24.03.2020 **Sivumäärä** 48 **Kieli** Englanti

Tiivistelmä

Hybridisaatioketjureaktio on tehokas tapa detektoida RNA:ta erinomaisella herkkyydellä. Sen detektionopeus ja -herkkyys on kuitenkin yleensä rajallinen, koska se on riippuvainen diffuusiosta. Ketjureaktion rajoittaminen pieneen tilaan johtaa nopeampiin detektioaikoihin ja tarkempaan herkkyyteen kuin rajoittamattomissa ketjureaktioissa, koska diffuusioilmiötä ei tarvita.

Tämän diplomityön tavoite on parantaa hybridisaatioketjureaktion detektionopeutta ja -herkkyyttä. Tavoitteena on yksinkertaistaa synteesiprosessia ja samalla voimistaa fluoresenssisignaalia. Tämän toteuttamiseksi käytettiin kahta DNA hiuspinnimonomeeria. Kun onnistunut hybridisaatioketjureaktio oli todennettu liuoksessa, DNA monomeerit kiinnitettiin nanopartikkeleihin. Hiuspinni-DNA:n kiinnittymistä tutkittiin ultraviolettivalon ja näkyvän valon spektroskopialla ja kiinnitys varmistettiin läpäisyelektronimikroskopialla. Hybridisaatioketjureaktiota nanopartikkelien pinnalla tutkittiin mittaamalla fluoresenssin intensiteetin muutosta.

Onnistunut hybridisaatioketjureaktio liuoksessa varmennettiin polyakryyliamidi geelielektroforeesin ja fluoresenssimittauksen avulla. Myös DNA:n onnistunut kiinnittyminen sekä pii- että kultananopartikkelien pinnalle todennettiin. DNA hiuspinnit olivat kuitenkin osittain auenneet kiinnittymisen jälkeen, mikä aiheutti ketjureaktion alkamisen ilman initiaatiotekijää. Aukeaminen varmennettiin polyakryyliamidi geelielektroforeesilla. Tästä huolimatta hybridisaatioketjureaktion todistettiin olevan mahdollinen nanopartikkelien pinnalla. Jotta menetelmästä tulisi käyttökelpoinen RNA:n detektointiin elävissä organismeissa, on menetelmää vielä optimoitava.

Avainsanat Hybridisaatioketjureaktio, kultananopartikkeli, piinanopartikkeli, pallomainen nukleiinihappo, RNA detektio

Preface

This master's thesis was carried out in the Research Group of Biohybrid Materials at the School of Chemical Engineering at Aalto University. The thesis project was very interesting and more challenging than I first thought. During the project I learned a lot and had to challenge my problem solving skills countless times.

First of all, I would like to thank professor Mauri Kostiainen for the opportunity to join his research group and learn about the academic world. The comments and suggestions you gave were extremely helpful. The biggest thanks of course goes to my advisor Qing Liu who guided me in my work and gave me continuous support and guidance throughout the project. I would also like to thank Antti Korpi for helping me with the DLS and zeta potential measurements, Ahmed for helping me with TEM imaging and Sofia Julin for providing her ideas when my work was in a standstill. Furthermore, I would like to thank all the members of the Biohybrid Materials Group for providing fun and supportive working environment. I also want to thank my family and friends for supporting me during all these years.

Contents

APPENDICES

Abbreviations and definitions

Abbreviation	Definition
3BHQ_1	3’-Black Hole Quencher® 1
3ThioMC3-D	3’-Thiol Modifier C3 S-S (Disulfide)
56-FAMN	5’-6-Carboxyfluorescein (NHS Ester)
5ThioMC6-D	5’-Thiol Modifier C6 S-S (Disulfide)
AAc	Acrylic acid
Ag	Silver
AgNP	Silver nanoparticle
APS	Ammonium persulfate
APTES	(3-aminopropyl)trimethoxysilane
AS	Ascorbate sodium
Au	Gold
AuNP	Gold nanoparticle
CdSe	Cadmium selenide
CHA	Catalytic hairpin assembly
DLS	Dynamic light scattering
DNA	Deoxyribonucleic acid
DMSO	Dimethyl sulfoxide
EDTA	Ethylenediamine tetraacetic acid
EtBr	Ethidium bromide
Fe_3O_4	Ferroso ferric oxide
GMBS	N-Succinimidyl 4-Maleimidobutyrate
H1	DNA hairpin 1
H2	DNA hairpin 2
HCR	Hybridization chain reaction
I	Initiator (Survivin RNA)
L1	DNA anchor 1
L2	DNA anchor 2

LSPR	Localized surface plasmon resonance
mRNA	Messenger RNA
NaCl	Sodium chloride
NaOH	Sodium hydroxide
NMWL	Nominal molecular weight limit
NP	Nanoparticle
PAGE	Polyacrylamide gel electrophoresis
PBS	Phosphate-buffered saline
PCR	Polymerase chain reaction
RNA	Ribonucleic acid
RCA	Rolling circle amplification
RCF	Relative centrifugal force
Si	Silicon
SiNP	Silicon nanoparticle
SNA	Spherical nucleic acid
$Si(OH)_4$	Orthosilicic acid
TBE	Tris/Borate/EDTA
TCEP	Tris(2-carboxyethyl)phosphine
TEM	Transmission electron microscopy
TEMED	Tetramethylethylenediamine
UV	Ultraviolet
UV/Vis	Ultraviolet-visible (spectroscopy)

1. Introduction

In vivo detection of RNA is of vital importance in the diagnosis of some serious diseases [1, 2]. Survivin is an apoptosis inhibitor protein and acts together with the mitotic spindle apparatus to regulate cell inhibitors and chromosomal segregation [3]. It is one of the most specific and ubiquitous molecules related to cancer identified so far. Survivin expression is uncommon in normal fully differentiated tissues in adults but most cancers, regardless of lineage, differentiation, and histologic type, overexpress survivin. This suggests reactivation of the gene and a potential target for drug therapy. [4] Thus, strategies targeting this protein via small-molecule inhibitors and specific immunologic approaches could offer promising treatment approaches in the future [5].

In 2004, Niles Pierce and Robert Dirks first demonstrated how binding of DNA to a substrate can realize both recognition and signal amplification without any external inputs [6]. This was realized by the triggered self-assembly of DNA nanostructures in a procedure called hybridization chain reaction (HCR). [6, 7] DNA hybridization chain reaction is a nonenzymatic catalytic amplification strategy with excellent sensitivity. It has shown excellent capability in the detection of RNA both *in vitro* and *in vivo*. [8, 9] In its simplest form the HCR works by storing potential energy in two stem-loop species. When an initiator is added to the stable mixture, one of the stem-loops opens, exposing new single-stranded region that opens a stem-loop of the other species (Figure 1.1). The second stem-loop has a single-stranded region alike the initiator which induces a chain reaction and the formation of a nicked double helix. [6, 7]

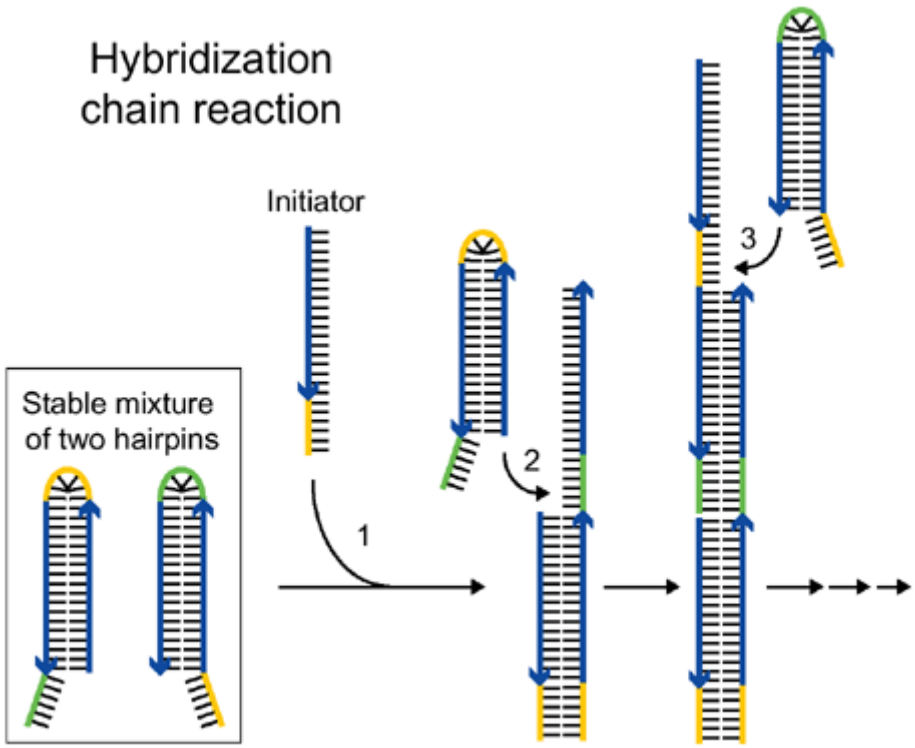

Figure 1.1. Schematic of a basic hybridization chain reaction. 1. Addition of initiator strand. 2 and 3. Hairpin species open in turn and hybridize to a chain. Reprinted from [7].

Not long ago, a DNA “nano string light” was fabricated and used for the detection of survivin mRNA. The two DNA stem-loops were restrained on a DNA template in close space and thus no diffusion process was needed. This led to 6.7 times faster detection speed than non-restrained chain reactions. [10] In another study, six reactant hairpins were constrained on a DNA origami, leading to a higher detection speeds [11]. In this project, we propose to further expand this concept to spherical nucleic acids. We aim to simplify the synthesis process while strengthening the fluorescence signal, thus creating a fast and robust tool for RNA detection.

This thesis is divided into six sections. Chapter 1, the introduction, presents the background and relevance of the study. Chapters 2 and 3 are the literature study of the thesis. The structure and properties of DNA and spherical nucleic acids, as well as characteristics of silicon and gold nanoparticles are presented in Chapter 2. Signal

amplification methods based on hybridization chain reaction are presented in Chapter 3. Chapters 4 and 5 form the experimental part of the thesis. In chapter 4, the materials and methods used in the study are presented and the conducted experiments are explained in details. Chapter 5 presents the results and discussions obtained in this work. Finally, in Chapter 6, conclusions are drawn, and suggestions for future research are proposed.

2. Spherical nucleic acids

Spherical nucleic acids (SNAs) are structures that are an arrangement of densely packed, highly oriented nucleic acids in a spherical geometry. They were first introduced by Mirkin *et al.* in 1996. [12] This chapter gives an introduction to the structure and properties of DNA and explains what makes them suitable for creating exquisite nanoscale structures. In addition, silicon nanoparticles (SiNPs) and gold nanoparticles (AuNPs) are examined as the core of the spherical nucleic acids.

2.1 Deoxyribonucleic acid

Deoxyribonucleic acid (DNA) is a polynucleotide built up from covalently linked deoxyribonucleotide units (nucleotides) and is widely known as the carrier of genetic information [13]. The nucleotide consists of a five-carbon sugar 2'-deoxyribose, a nitrogenous base, and a phosphate group. The base is a derivative of either bicyclic purine or monocyclic pyrimidine. The purine bases are adenine (A) and guanine (G), whereas the pyrimidine bases are cytosine (C) and thymine (T). 3', 5'-phophodiester bonds covalently link the nucleotides from the 5'- hydroxyl group of one nucleotide to the 3'-hydroxyl group of the adjacent one. This results in an alternating sugar and phosphate diester, which forms the backbone of DNA. The negatively charged phosphate groups give the DNA as a whole a negative charge (Figure 2.1A). Due to the free 5'-phosphate and 3' -hydroxyl groups at the opposite ends of the strand, DNA also has polarity. [14, 15]

Double helical structure is the principal secondary structure of DNA. It forms when two DNA single strands with complementary base sequences hybridize together. [12, 16]. Hydrogen bonds between complementary strands and base stacking interactions between adjacent base pairs are the main reasons why the DNA double helix is held

together. Hydrophobic interactions and electrostatic forces also help in stabilizing the DNA structure.[17-19]. The adenine pairs efficiently through two hydrogen bonds with thymine while cytosine bonds to guanine with three hydrogen bonds (Figure 2.1B). The two DNA strands have to be antiparallel to each other for the formation of well aligned hydrogen bonds. [15, 20]

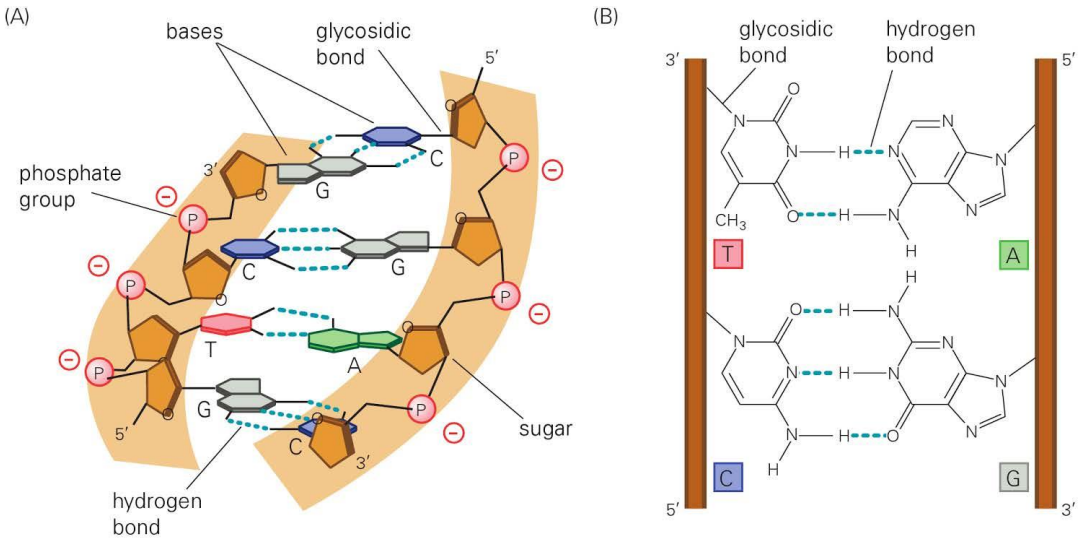

Figure 2.1. The structure of DNA. a) DNA strand has a negatively charged backbone consisting of alternating sugar and phosphate diester. b) Hydrogen bonds between the Watson-Crick base pairs link two DNA single strands together to a double helical structure. Reprinted from reference [16].

The base stacking interactions stabilize the structure by permitting the bases to stack on top of each other, which minimizes the contact of the bases with surrounding phase. The interactions are mainly van der Waals and dipole-dipole interactions. [14, 21]. The strength of the hydrogen bonds depends on the base pair and are considerably weaker than the base stacking interactions. The two hydrogen bonds formed between adenine and thymine have in vacuum a stabilization energy of $E_{A\text{-}T}$ = 25 kJ/mol, and the equivalent value for the three hydrogen bonds formed between cytosine and guanine is $E_{C\text{–}G}$ = 46 kJ/mol [16]. Hence, the more C-G base pairs a DNA double helix contains, the more stable it will be against pH and thermal mediated denaturation into initial single strands [22, 23]. Furthermore, chain length, sequence

and salt concentration influence the DNA duplex denaturation. This means it likewise influences the melting temperature of double-stranded DNA [23].

The most attractive properties of DNA are its programmability, self-assembly, and predictability. Many unique nanoscale structures and complex devices have been reported since the first demonstration of creating lattices from a finite set of DNA sequences. [24-27] Two main research themes are being scrutinized in the field of DNA nanotechnology: structural DNA nanotechnology and dynamic DNA nanotechnology. In the structural DNA nanotechnology, nanoscale architectures are created with molecular self-assembly via hybridization, which can be further expanded into microscale structures. [28] In dynamic DNA nanotechnology, programmable dynamic nanomachines like DNA strand displacement systems are utilized in the creation of molecular motor and performing primitive computations. [29]

2.2 Silicon nanoparticles

Silicon (Si) is a semiconductor and has been well studied. It is abundant in the Earth. The fascinating properties, including stability, loading capacity and biocompatibility, have greatly boosted the development of silicon nanoparticles (SiNPs) for bio-medical applications. They can also exhibit effective visible emission thanks to their suitable surface modification favoring the radiative recombination and the quantum confinement effect. [30-34] SiNPs are dielectric nanoparticles, which can have both electric and magnetic dipole resonances simultaneously excited inside the same particle [35-37], which is in contrary to spherical metallic nanoparticles that triggers resonant scattering through electric-type resonances [38]. The magnetic dipole response of dielectric particles arises from the circular displacement currents excited inside the particle by incident light [39].

There are numerous methods by which SiNPs can be produced, such as laser-driven pyrolysis of silane [40, 41], ultrasonic dispersion of electrochemically etched silicon [42], gas phase synthesis [43], microemulsion synthesis [44] and many more [45-53]. Surface modification is a crucial factor in the preparation of SiNPs for biological applications and most of the methods listed above produce hydrophobic SiNPs [54]. Studies describing methods of creating water-dispersible SiNPs for biological applications are limited but there are a few of them [52-54]. Such methods include lateral electrochemical anodization [52], UV-induced graft polymerization of acrylic acid (AAc) on the surface of SiNPs [53], and simple synthesis by facile mixing and stirring the reagents (3-aminopropyl)trimethoxysilane (APTES) and ascorbate sodium (AS) under room temperature for 30 min [54].

SiNPs present an attractive chemical alternative over heavy metal-containing quantum dots for *in vivo* application. Heavy metal-containing quantum dots have been shown to be toxic in biological environments, while silicon is already a common trace element in humans. Orthosilicic acid ($Si(OH)_4$), the biodegradation product of porous silicon, is naturally found in various tissues and can be efficiently excreted from body through urine. [55, 56]

2.3 Gold nanoparticles

Gold nanoparticles (AuNP) have drawn increasing interest in the field of nanotechnology in the past few decades, mainly due to their unique electronic, optical, chemical and physical properties. AuNP properties are vastly different from individual gold (Au) atoms and bulk gold. [57, 58]

The appealing optical properties of gold and other metal nanoparticles arise from their localized surface plasmon resonance (LSPR). LSPR is the coherent oscillation of the conduction electrons induced by interaction with electromagnetic field, for example light. When AuNP dispersion is illuminated with visible light, strong

absorption of the light will occur at a certain wavelength which is dependent on the interparticle distance, particle size and shape, the presence and nature of a supporting or stabilizing ligand shell, and the dielectric constant of the dispersion medium. This absorption can be seen as a peak in the absorption spectrum and its origin is the collective oscillation of free surface electrons induced by the incoming light (Figure 2.2). [57-61] For small AuNPs with a diameter around 10-15 nm, the absorption peak is usually in the 520 nm region as a result of strong abortion of green light. This gives a characteristic ruby red color of the colloidal gold. [57-62] In 1908, Gustav Mie [63] explained the color of AuNPs and the LSPR by solving Maxwell's equation for the absorption and scattering of electromagnetic radiation with homogeneous spherical particle model.

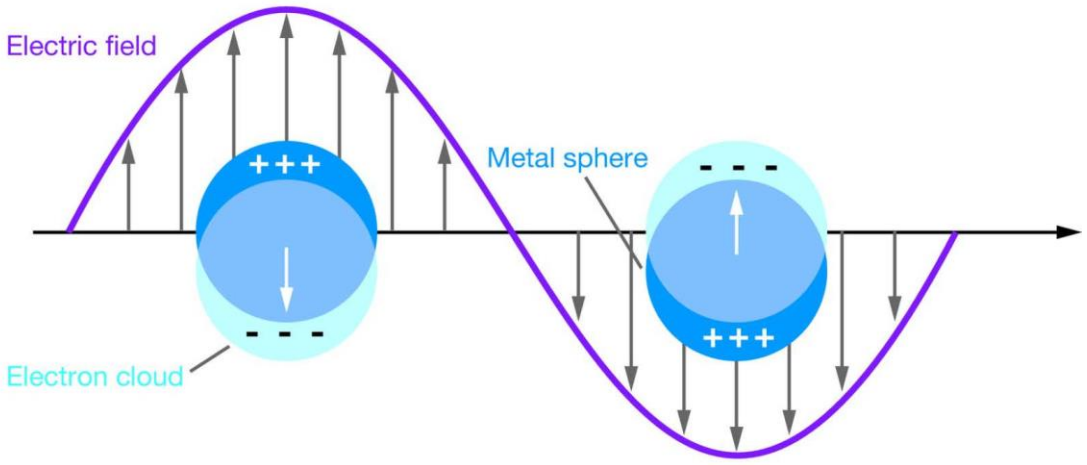

Figure 2.2. A schematic illustration of the localized surface plasmon resonance of metal nanoparticles. Reprinted from reference [64].

Both bottom-up and top-down approaches can be used in AuNP synthesis and the development of new, optimized synthesis routes have been ongoing in the recent years [57, 65-68]. The goal is to be able to synthesize AuNPs with narrow size distributions, different sizes and shapes and suitable surface functionalities for tailored applications. AuNPs have been already found use in array of nanotechnology applications like nanophotonic [69] and electronic [70] devices, biomedical analysis

tools [67, 71] and drug-delivery systems [67, 72]. In the future, they are promising in catalytic, electronic, optical, and sensing applications and are expected to be found in high-capacity drug delivery agents, solar cells, theranostic materials and many other applications [73]. The geometrical arrangement of AuNPs affects their optical and electronic properties vastly, which leads to the need of controlling and directing their arrangements and positions at the nanoscale level. [13, 74, 75].

2.4 Spherical nucleic acids

Spherical nucleic acids (SNAs) have attracted interest owing to the potential in cell transfections [76, 77], *in vitro* biodetection [78, 79], intracellular assays [80, 81], therapeutics [82], and gene regulation [77, 83]. First form of SNAs were made of gold cores and DNA shells [12]. The properties these types of conjugates exhibit are distinct from those of both the nanoparticles and DNA from which they derive [84]. Most forms of nucleic acids rely on the hybridized duplex as the fundamental structural unit that determines their overall shape. As for SNAs, they can be prepared from either single-stranded or double-stranded nucleic acids, and their orientation is determined by the shape of the inorganic cores. [85-87] The forms of nucleic acids and the modes of assembly of SNAs are presented in Figure 2.3.

The oligonucleotide shell is responsible for a great deal of SNAs' overall properties and governs its stability in complex media [84]. The properties the shell exhibits have been well studied and are predictable based on its structure [88, 89]. Oligonucleotides are usually designed with a suitable particle-attachment moiety, a spacer region, and a programmable recognition sequence. The most common attachment method to AuNP is based on bonds between Au and SH group at 5' or 3' end of DNA. The spacer region used to extend the active recognition portion of the oligonucleotide sequence away from the NP core usually contains around 10 nucleotides (~3 nm). The recognition strand depends on the technological use it is designed for and are usually available for further base-pairing with other strands of

interest. Furthermore, other functional groups such as quenchers, dye molecules, drugs, and modified bases can be attached along any position of the oligonucleotide. [84]

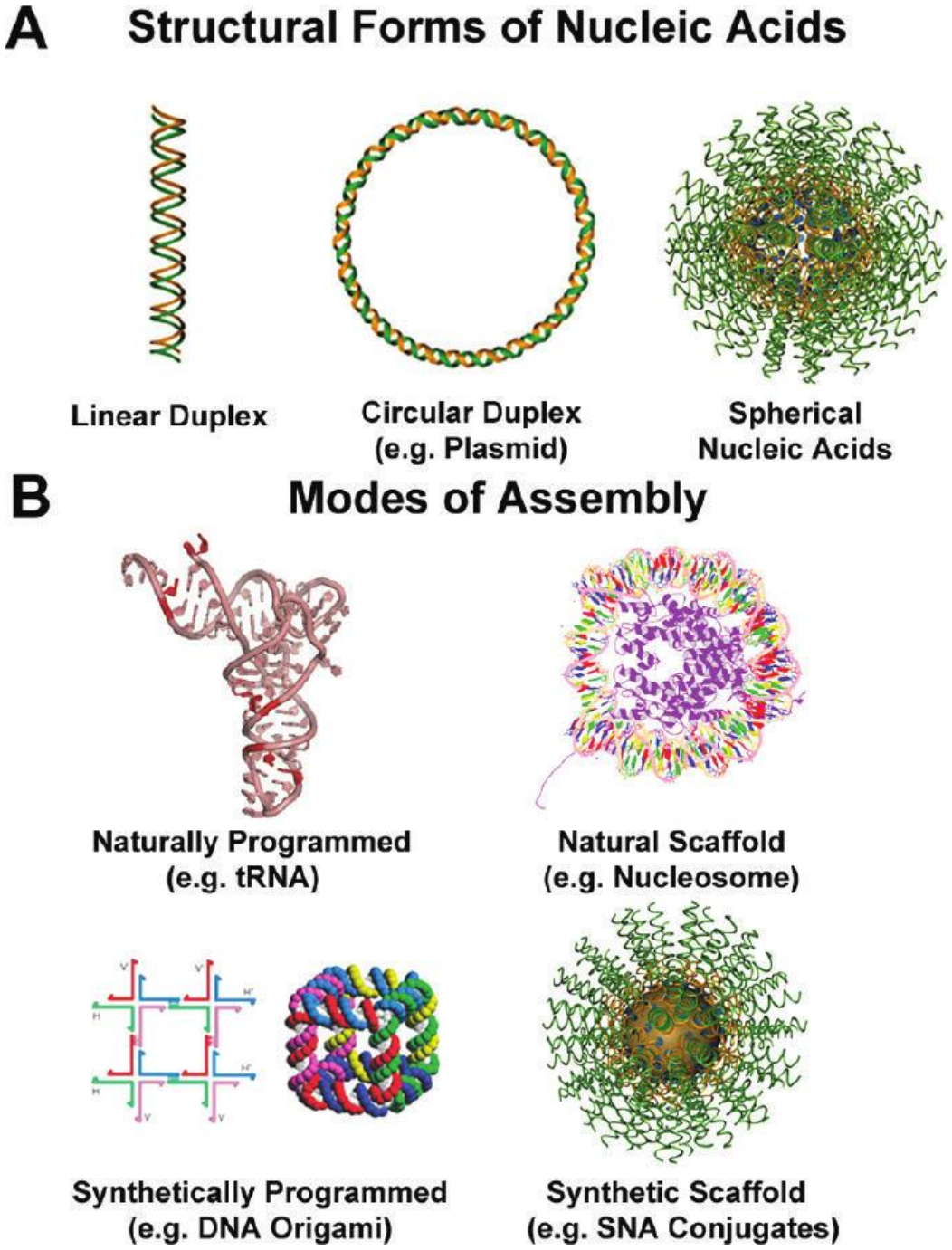

Figure 2.3. (A) Structural forms of nucleic acids. (B) Nucleic acid structures with well-defined shapes are made naturally through sequence selection and base-pairing interactions (top left) or through synthetic means (bottom left). Alternatively,

templates such as proteins (top right) or synthetic nanostructures (bottom right) can be used to make highly functional architectures based on the size and shape of the template. Reprinted from reference [84].

The core materials of SNAs is a way to tailor the behavior SNA conjugates. The physical and chemical characteristics of core materials differ greatly, such as gold (Au) [12], silver (Ag) [90], ferroso ferric oxide (Fe_3O_4) [91], cadmium selenide (CdSe) [92], and silicon (Si) [34]. Each particle requires specific chemistry to attach oligonucleotides, which is a nontrivial task due to the oligonucleotide densities necessary to achieve the properties unique to SNAs [84]. AuNPs as a core can be easily functionalized with a wide variety of chemical reagents and can be synthesized over a range of diameters [84, 93]. Aqueous AgNPs are easily oxidized and for this reason are typically prepared from oligonucleotides with multiple cyclic disulfide anchoring groups [90, 94]. CdSe quantum dots have been functionalized via a three-step process that entails ligand exchange, solvent exchange, and incubation with alkylthiol-functionalized oligonucleotides [92]. SiNPs have to be surface modified to attach oligonucleotides. For example, maleimide modified SiNPs can be incubated with alkylthiol-functionalized oligonucleotides while azide-functionalized SiNPs can be modified with alkyne-modified oligonucleotides [95, 96].

The amount of DNA that can be attached on NPs depends on the particle size and shape. For spherical particles, the smaller they are the higher densities they can support. With bigger particles the maximum surface coverage approaches that of planar materials. The density of DNA affects greatly the properties of SNAs. [84] For example, comparing to free DNA duplex, the melting transition of gold particle-bounded duplexes occurs at higher temperatures because of the properties of the dense SNA shell. For silica SNAs the melting transition is similar to that of free duplexes due to low DNA density (1/30 of AuNP SNA). [84, 97] Gold core can also be used as a scaffold to cross-link DNA. After dissolving the gold core, a coreless form of SNAs can be obtained. These SNAs display many of the properties of the original AuNP conjugates, like the ability to efficiently transfect cell membranes without the

need for co-carriers and cooperatively hybridize with complementary nucleic acids. [98]

There is still much we don't understand about SNAs. Their scope of utility, fundamental properties, and the diversity of possible conjugate materials are all still under investigation. Their modes of intracellular trafficking at the molecular level, the route they move from cell to cell within living systems, and the reason that they can penetrate tissues and organs much more effectively than analogous molecular systems are not fully understood. In the future, SNAs are expected to be used in life sciences, catalysis, electronics, storage, and energy harvesting and conversion. [84] For those who wish to have even a better understanding of SNAs, an article by Cutler *et al.* [84] is recommended.

3. Hybridization chain reaction

Detection of biomolecules in living cells remains challenging owing to their low expression level and the complex intracellular environment [99]. But it is of vital importance for the diagnosis of some serious diseases [1, 2]. As a nonenzymatic catalytic amplification strategy, DNA hybridization chain reaction (HCR) is a powerful tool with excellent sensitivity and has already shown great potential in the detection of RNA *in vitro* and *in vivo* [8, 9].

3.1 Amplification techniques

To detect low-abundance nucleic acids in complex media, amplification methods are needed. Polymerase chain reaction (PCR) is the most common amplification method for amplifying and detecting minute quantities of nucleic acids. It has been broadly used in numerous fields but requires large and expensive thermal cyclers, limiting its applications in settings where resources are limited [100]. Another common technique for the amplification is rolling circle amplification (RCA) [101]. These methods have assisted ultrasensitive biosensing of numerous targets such as proteins, RNA, and small molecular biomarkers. However, both aforementioned techniques require exotic enzymes, which hinders their application inside living cells [102].

Enzyme-free catalytic amplification strategies based on DNA cascade reaction don't need exotic enzymes during the reaction process. Thus, they have become important tools for biomolecule detection both *in vitro* and *in vivo*. [103-105] Such amplification strategies include hybridization chain reaction (HCR) and catalytic hairpin assembly (CHA). [6, 106, 107]

3.2 Principles and mechanisms

Hybridization chain reaction (HCR) is based on at least two nucleic acid hairpin species that are designed to remain as monomers in the absence of nucleic acid initiator (I) [6]. Each nucleic acid hairpin consists of input domain with an exposed single-stranded toehold and an output domain with a single-stranded toehold sequestered in the hairpin loop [108]. When the initiator is introduced, it will hybridize to the input domain of one of the hairpin structures, open the hairpin and expose its output domain which is complementary to other hairpins' input domain [6, 108]. The HCR will generate a chain reaction of alternating hairpins until the hairpins are exhausted, polymerizing into a long, nicked double-stranded DNA molecules [6, 108, 109]. This reaction is presented in Figure 3.1.

Usually, the speed of HCR is limited by the speed of diffusion kinetics. Diffusion happens in three-dimensional fluidic space where DNA molecules randomly collide and interact. The collision frequency depends on the concentration and temperature of the system. With too low concentrations and temperatures the kinetics of the systems could be impeded due to the low collision frequency. At higher concentrations and temperatures, unintended interactions increases the amount of leaks, which means that the hybridization reactions happen in the absence of input strands. [8-10]

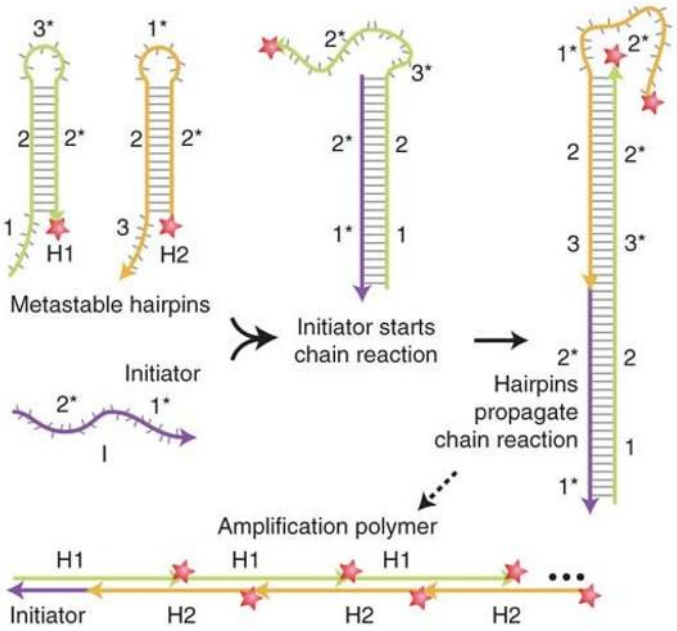

Figure 3.1. Schematic of the hybridization chain reaction. Reprinted from reference [108].

Several works have shown that confining successive reactants together leads to faster reaction rates [10, 11, 110-112]. This maintains high local concentrations of hairpins, promotes substrate transportation, protects them against damage, and accelerates reaction [113-116]. The hairpins have to be far enough so that the two domains cannot reach each other until the first hairpin is opened, but still close enough so that they can reach after the ring opens [11]. One example of the confined reactants is the study done by Ren et al. They hybridized the successive hairpins to a DNA nanowire. The confined hybridization chain reaction was named DNA cascade reaction (DCR) and the system was called a responsive DNA “nano string light” (DNSL). Such confinement leads in their case to a 273-fold increase in local concentration, which in succession leads to a 6.7 times faster reaction time. The fluorescence spectra and the schematic of the reaction in the study can be seen in Figure 3.2.

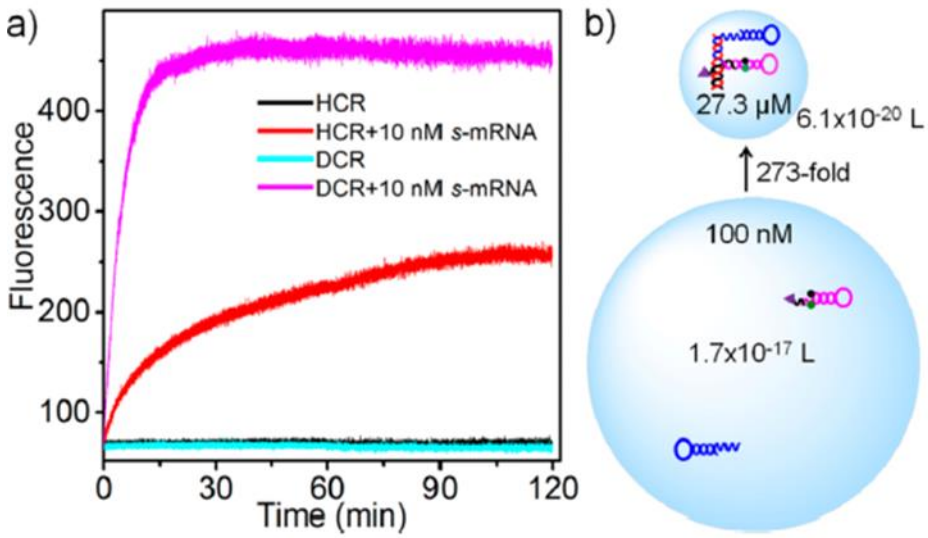

Figure 3.2. a) Fluorescence spectra of DCR and HCR in homogenous solution. b) The reaction area and local concentration for DCR and HCR. Reprinted from reference [10].

4. Materials and methods

In this thesis, the hybridization chain reaction on the surface of spherical nanoparticles is studied in order to establish a fast and ultrasensitive tool for RNA detection. In this chapter, the design of the DNA hairpins and methods used for sample preparation and characterization are presented.

4.1 DNA hairpin designs

This part describes the designs of the DNA hairpins for SiNPs and AuNPs.

4.1.1 DNA hairpins for SiNPs

The sequences of the DNA hairpins for SiNPs attachment were adapted from Bui *et al.* with minor modification [11]. Both hairpins contain a stem, a loop and a sticky end. Two anchor DNAs, L1 and L2 with thiol group, were used to attach to SiNPs through thiol-maleimide bond, followed by the hybridization of hairpins H1 and H2 to L1 and L2, respectively. The sequences of all the DNAs including the survivin DNA initiator are presented in Table 4.1. The color coding shows the complementary regions of the DNAs and corresponds to the colors indicated in Figure 4.2.

Table 4.1. DNA sequences used for SiNPs. The color coding shows the complementary regions and corresponds to the colors used in Figure 4.2.

DNA type	Sequence	Bases
Survivin	5'-TCT CAA GGA CCA CCG CAT CTC TAC-3'	24
H1	5'-/56-FAMN/TGG ACC ACC GCA TCT CTA CCG AAG TTT TTT TTT TTG TAG AGA TGC GGT GGT CCT TGA GAC TGG TCC ATT TGT A-3'	73
H2	5'-CCT CGC TCG GCT ATA CTT CGG TAG AGA TGC GGT GGT CCT TTT TTT TTT TCT CAA GGA CCA CCG CAT CTC TAC-3'	72

L1	5'- /5ThioMC6-D/TTT TTT TTT TTT TAC AAA TGG ACC AG/3BHQ_1/-3'	26
L2	5'- ATA GCC GAG CGA GGT TTT TTT TTT TT/3ThioMC3-D/-3'	26

The formation of DNA hairpins and the hybridization of H1 to L1 and H2 to L2 in 3 concentrations was evaluated and are listed in Table 4.2. The samples were subjected to thermal-annealing ramp (G-storm G1 Thermal Cycler) for full hybridization: all samples were first heated to 95 °C and incubated for 15 minutes and then cooled from 95 °C to 4°C over the course of 92 minutes (-1 °C/min). After annealing, the DNA was stored at 4 °C until the program was manually stopped.

Table 4.2. The samples prepared for the hybridization check.

Sample	H1 or H2	L1 or L2	Volume	Final concentration
H1	100 pmol	100 pmol	50 µl	2 µM
H2	100 pmol	100 pmol	50 µl	2 µM
H1L1	50 pmol	50 pmol	50 µl	1 µM
H1L1	100 pmol	100 pmol	50 µl	2 µM
H1L1	250 pmol	250 pmol	50 µl	5 µM
H2L2	50 pmol	50 pmol	50 µl	1 µM
H2L2	100 pmol	100 pmol	50 µl	2 µM
H2L2	250 pmol	250 pmol	50 µl	5 µM

Polyacrylamide gel electrophoresis (PAGE) was used to check DNA hybridization and HCR. Gel electrophoresis is a widely used technique to separate nucleic acid fragments by size. When an external electric field is applied, the negatively charged DNA fragments will migrate through the polyacrylamide gel matrix towards the anode. But since larger fragments will be retarded by the pores in the gel matrix, the fragments will be separated based on size and shape [117]. In this case, the gel electrophoresis will separate the hybridized DNA strands from non-hybridized DNA strands. Ethidium bromide (EtBr) was used as a fluorescent tag for DNA imaging. EtBr binds to DNA by intercalating between stacked base pairs and the fluorescence can be clearly recorded when exposed to ultraviolet (UV) light [117].

For the PAGE, a 15 % (m/v) polyacrylamide gel was made by mixing 3.8 ml H_2O, 2 ml 5× Tris/Borate/Ethylenediaminetetraacetic acid (EDTA) (TBE) buffer, 3.8 ml 40 % acrylamide/bis solution (19:1), 400 µl 3wt % Ammonium persulfate (APS) solution and 15 µl tetramethylethylenediamine (TEMED). The polymerization takes about 30 min. DNA samples were prepared by mixing 5 pmol of DNAs in 5 µl of PBS with 5 µl 2× TrackIt™ Cyan/Yellow Loading Buffer (Thermo Fisher Scientific). The whole solution of 10 µl was loaded into the gel wells. TrackIt™ Ultra Low Range DNA Ladder (Thermo Fisher Scientific) was used as a reference after it was 2× diluted. During the gel electrophoresis, 1×TBE was used as a running buffer and the voltage applied was increased stepwise: 90 V for 20 minutes, 120 V for 20 minutes and 150 V for 20 minutes. A BioRad PowerPac™ Basic with the BioRad Mini-PROTEAN® Tetra System was used for the electrophoresis. The gel was stained by incubating with a small amount of EtBr for 15 minutes in 1× TBE buffer. After that, the gel was visualized under UV light using a BioRad Gel Doc Ez Imager.

4.1.2 DNAs for gold nanoparticles

Two DNA hairpins, GH1 and GH2, (Sequences in Table 4.3) were used in this study. They are a bit different from the ones used for SiNPs as they do not contain the sticky ends. A fluorescent dye (FAM) was attached to the 3' of GH1.

Table 4.3. DNA sequences used in this study for AuNPs. The color coding shows the complementary regions of the hairpins and corresponds to the colors used in Figure 4.2.

DNA type	Sequence	Bases
Survivin	5'-TCT CAA GGA CCA CCG CAT CTC TAC-3'	24
GH1	5'-/56-FAM/TGG ACC ACC GCA TCT CTA CCG AAG TTT TTT TTT TTG TAG AGA TGC GGT GGT CCT TGA GA/3ThioMC3-D/-3'	59
GH2	5'-/5ThioMC6-D/ACT TCG GTA GAG ATG CGG TGG TCC TTT TTT TTT TTC TCA AGG ACC ACC GCA TCT CTA C-3'	58

The design for the fluorescence quenching was designed based on the study of Guillermo *et al.* [118]. As shown in Figure 4.1, the quenching effects of 10 nm AuNP on fluorophore are strongly influenced by the distance between components. In our design, the distances between FAM and AuNP were estimated to be around 3 nm and 12 nm before and after the ring opening (Figure 4.2). In this case, the relative fluorescence intensity should rise from almost zero to around 0.7, which can be regarded a dramatic increase for future application.

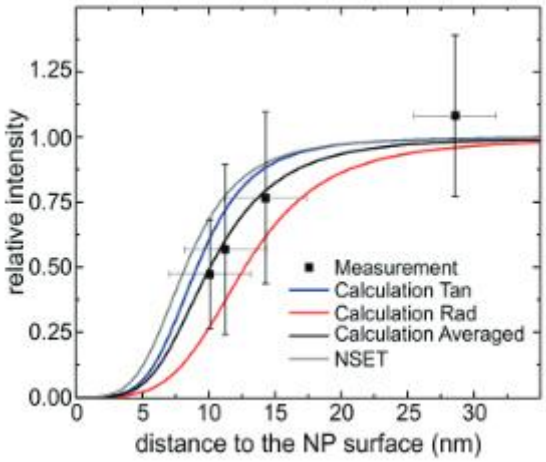

Figure 4.1. Relative change in fluorescence intensity based on distance on the surface of 10 nm AuNPs. Reprinted from reference [118].

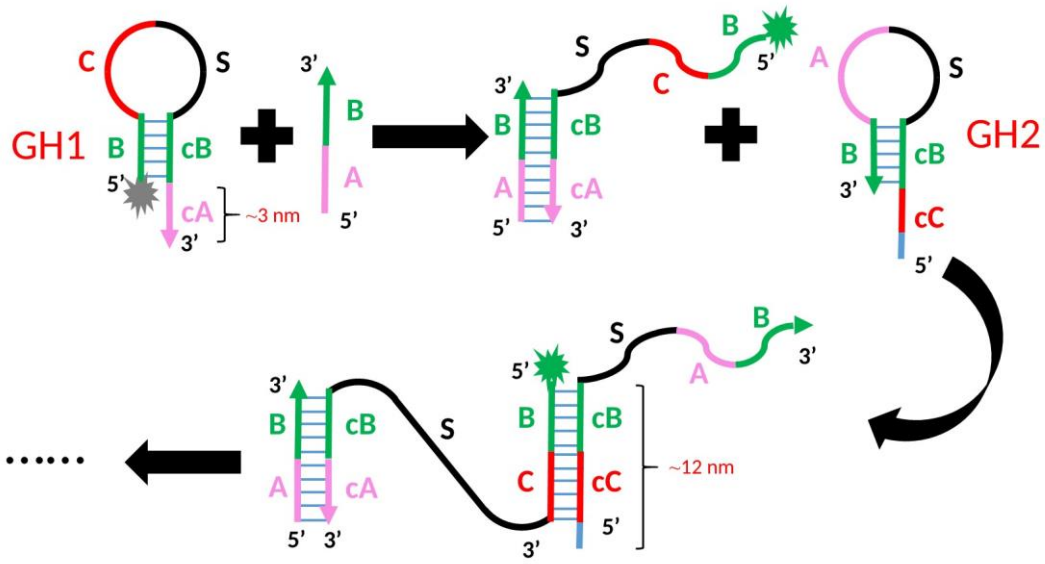

Figure 4.2. The design for DNA hairpins, GH1 and GH2, and schematic of the progression of hybridization chain reaction. The color coding corresponds to the sequence region stated in Table 4.1.

4.2 Hybridization chain reaction in solution

The hybridization chain reaction was tested in PBS solution before the attachment of DNA to nanoparticles. The chain reaction was tested with PAGE and time-dependent fluorescence spectra. In Figure 4.3, a schematic of the chain reaction progress is shown. Without the initiator both of the DNA stem-loops should stay unopened and with the introduction of the initiator the chain reaction should start rapidly.

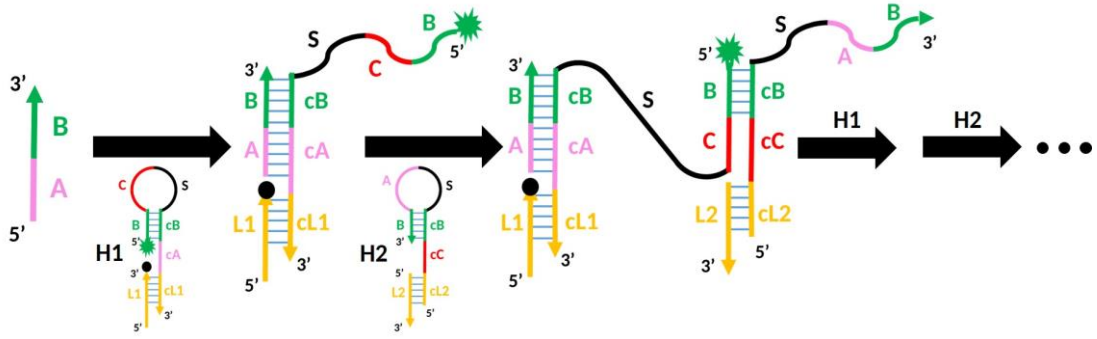

Figure 4.3. Schematic of the progression of HCR. The color coding corresponds to that in Table 4.3.

The DNAs used for samples were first subjected to thermal annealing similarly as described before. After annealing, corresponding DNAs were mixed for gel electrophoresis, as shown in Table 4.4

Table 4.4. The samples prepared for gel electrophoresis.

Sample	H1L1	H2L2	I	Volume
H1L1	5 pmol			20 µl
H2L2		5 pmol		20 µl
H1L1+I	5 pmol		5 pmol	20 µl
H2L2+I		5 pmol	5 pmol	20 µl
H1L1+H2L2	10 pmol	10 pmol		20 µl
H1L1+H2L2+I (50%)	10 pmol	10 pmol	5 pmol	20 µl
H1L1+H2L2+I (100%)	10 pmol	10 pmol	10 pmol	20 µl
H1L1+H2L2+I (200%)	10 pmol	10 pmol	20 pmol	20 µl

For the time-dependent fluorescence spectra measurement, samples were prepared in a 96-well polystyrene microplate without a lid (Thermo Scientic™ Nunc™ MicroWell™) with 100 nM concentrations in 100 µl PBS. The measurement was carried out using a BioTek™ Cytation™ 3 Cell Imaging Multi-Mode Reader using excitation wavelength of 488 nm and the emission wavelength of 520 nm was recorded every 50 seconds for 3 to 5 hours.

4.3 DNA hairpin attachment on silicon nanoparticles

This part describes the functionalization and attachment of the DNAs on SiNPs.

4.3.1 SiNPs functionalized with maleimide

N-Succinimidyl-4-Maleimidobutyrate (GMBS) was used as a cross-linker to endow SiNPs with maleimide group. The amine modified SiNPs were first sonicated into homogeneous dispersion for half an hour. 1 ml SiNPs (10 mg/ml) in ethanol was taken and centrifuged with Eppendorf™ 5424R Microcentrifuge at 5000 RCF for 5 minutes to remove the ethanol. Then, SiNPs were washed with phosphate-buffered saline

(PBS) 3 times and resuspended in 900 µl PBS. To this solution 5 mg GMBS in 100 µl dimethyl sulfoxide (DMSO) was added and the mixture was left for shaking at room temperature overnight. After the reaction, excess GMBS was washed away using PBS with centrifugation at 2000 RCF for 2 minutes for 4 times. Afterwards the SiNPs were resuspended in PBS at 10 mg/ml.

Successful maleimide modification was determined by dynamic light scattering (DLS) and zeta potential measurement. The DLS measurements were performed using a Zetasizer Nano ZS (Malvern Instruments Ltd) equipped with a He-Ne ion laser at a wavelength of 633 nm. The measurements were carried out at 25 °C and the scattered light was detected at an angle of 173° (backscattering) with laser attenuation and measurement position adjusted automatically by the Malvern software. The diameter was determined from intensity-based particle distribution and a refractive index of 1.45 and an absorption index of 0.01 were used for distribution estimation. The measurements were performed in disposable Brand® micro UV-cuvettes, with each sample consisting of 100 µl 1 mg/mL SiNPs aqueous solution. Three measurements of 10 runs with 5 s duration was performed for each sample, and the diameter was obtained as the average of three measurements [119].

The zeta potential was measured using the same Zetasizer Nano ZS (Malvern Instruments Ltd). The measurements were carried out at 25 °C with refractive index of 1.45 and absorption index of 0.01. The measurements were performed in disposable Folded Capillary cell DTS1070 (MalvernPanalytical) and each sample consisted of SiNPs in 750 µl aqueous solution in 1 mg/ml concentration. Three measurements of automatic 10-100 runs with 30 s duration was performed for each sample and zeta potentials were obtained from apparent zeta potentials as the average of three samples.

4.3.2 DNA attachment to SiNPs

Two different methods of attaching the DNAs to SiNPs were used. In the first method, the DNA attachment to the SiNPs was done in two parts. First, the anchor DNA was deprotected. The deprotection of anchor DNAs was done by adding 20× excess of tris(2-carboxyethyl)phosphine (TCEP) in PBS with pH between 7 and 8. The deprotection reaction was carried out for one hour at room temperature with 1200 rpm shaking in an Eppendorf ThermoMixer® C. Afterwards, the excess amount of TCEP was removed using centrifugal filters (Amicon®Ultra 0.5ml Centrifugal Filters, 10 000 NMWL, Merck Millipore Ltd.) at 14000 RCF for 5 minutes at 4 °C. This was repeated 3 times and each time 200 µl of PBS was added. The deprotected anchor DNA was then mixed with maleimide modified SiNPs and left react overnight at room temperature. After the coupling, excess amount of DNA was then washed away 4 times by centrifuging at 2000 rpm for 2 minutes. The corresponding DNA hairpins in PBS were subjected to thermal-annealing and then mixed with the DNA anchor containing SiNPs in PBS. The mixture was left for hybridization at room temperature overnight. Afterwards, excess amount of DNA was washed away with centrifugation for 4 times.

In the second method, the anchor DNAs and corresponding DNA hairpins were first subjected to thermal-annealing for hybridization. After that, the hybridized DNAs were deprotected similarly as described before. Next, deprotected DNAs were mixed with the maleimide modified SiNPs and reacted overnight at room temperature. After the coupling, excess DNAs were washed away were washed away for 4 times.

4.4 DNA hairpin attachment on gold nanoparticles

The process for attaching the DNAs on gold nanoparticles was adapted from Ijäs *et al.* [120]. Before starting the attachment process, the GH1 and GH2 were first subjected to thermal-annealing and deprotection with TCEP as described before. The deprotected samples were washed with 10 mM Phosphate buffer (PB).

The DNA attachment protocol were carried out at 40 °C with constant shaking of 600 rpm. First, 20 µl of AuNPs was incubated with 0.4 µl of 1 % SDS water solution for 20 min. Then 200 pmol of DNAs were added in lowest amount of PB possible and incubated for half an hour. In the salting process, 3.2 M NaCl was added in 2 minute intervals for 18 times. The amount of NaCl added each time was adjusted to keep the NaCl concentration in the samples roughly the same as reported by Ijäs *et al.* [120] throughout the salting process. After the salting, DNAs with AuNPs were incubated for 1 h. Afterwards, excess DNA was washed away by spin-filtration (Amicon®Ultra 0.5 ml Centrifugal Filters, 100 000 NMWL, Merck Millipore Ltd.) by centrifuging at 14000 RCF for 10 minutes at RT. The washing step was repeated 4 times and in each filtration step 200 µl of PBS was added. The supernatants from the filtrations were collected to measure the amount of unreacted DNAs.

4.5 Analyzing the DNA on nanoparticles

The attachment of the DNAs on nanoparticles were calculated according to DNAs measured in the supernatant. The concentrations of DNA in the supernatant were measured using an UV/Vis spectroscopy. The absorbance at a wavelength of 260 nm was measured with a BioTek Eon Microplate spectrophotometer using a Take3™ micro-volume plate with a sample size of 2 µl. Calibration cures were plotted for the determination of DNAs concentrations in the supernatants.

The presence of DNA on the surface of the SiNPs was also confirmed by transmission electron microscopy (TEM) using a FEI Tecnai 12 Bio-Twin instrument operated at an acceleration voltage of 120 kV. The samples were stained before the TEM imaging to make the DNA visible and the protocol for the sample preparation was adapted from Castro *et al.* [121]. The samples were prepared on plasma cleaned (20 seconds oxygen plasma flash) Formvar carbon coated copper grids (Electron Microscopy Science). First, 3 µl of DNA coated SiNP solution was applied onto the carbon-coated

side of the TEM grid and excess sample solution was blotted away with filter paper after an incubation of 3.5 minutes. The samples were then negatively stained using a 2 % uranyl formate stain solution containing 25 mM sodium hydroxide (NaOH). Next, the sample-side of the grid was immersed into a 5 µl stain solution droplet. The stain was blotted away with filter paper immediately and the sample side of the grid was immersed into another droplet of 20 µl of stain solution. Excess stain solution was blotted away with filter paper after 45 seconds. After these procedures, the samples were left to dry under ambient conditions for half an hour before imaging.

4.6 Hybridization chain reaction on nanoparticles

The hybridization chain reaction of DNA on the surface of nanoparticles (NPs) was performed similarly as those without nanoparticles and samples without SiNPs or AuNPs were used as reference. All the sample prepared for the measurements are presented in Table 4.5. The samples were measured with Cytation 3 in a 96-well polystyrene microplate without a lid using excitation wavelength of 488 nm and recording emission wavelength of 520 nm.

Table 4.5. Samples for the hybridization chain reaction on SiNPs.

Sample	DNA conc.	Initiator conc.	Volume
PBS	0	0	100
H1	100 nM	0	100
H1L1	100 nM	0	100
H2L2	100 nM	0	100
H1L1+I	100 nM	10 nM	100
H1L1+H2L2+I	100 nM	10 nM	100
SiNPs with H2L2	100 nM	0	100
SiNPs with H2L2+I	100 nM	10 nM	100
SiNPs with H1L1 and H2L2	100 nM	0	100
SiNPs with HIL1 and H2L2+I	100 nM	10 nM	100

For HCR on AuNPs measurement, one more control sample was added: free H1 mixed with AuNPs in the solution. This was used to test the effect the AuNPs have on the

fluorescence when DNA and AuNPs are not bonded in the solution. The samples are presented in Table 4.6 and were measured with Cytation 3 in a 96-well polystyrene microplate without a lid using excitation wavelength of 488 nm and recording emission wavelength of 520 nm.

Table 4.6. Samples for the hybridization chain reaction on AuNPs.

Sample	DNA conc.	Initiator conc.	Volume
PBS	0	0	100
H1	100 nM	0	100
H2L2	100 nM	0	100
H1+AuNPs	100 nM	0	100
GH1 on AuNPs	100 nM	0	100
GH2 on AuNPs	100 nM	0	100
GH1 and GH2 on AuNPs	100 nM	0	100
GH1 on AuNPs+I	100 nM	10 nM	100
GH2 on AuNPs+I	100 nM	10 nM	100
GH1 and GH2 on AuNPs+I	100 nM	10 nM	100

5. Results and discussion

This chapter outlines the main results obtained within the scope of this thesis.

5.1 DNA hairpin formation check

PAGE was used to verify the formation of DNA intramolecular hairpins and the hybridization between DNA hairpins and corresponding DNA ligands. The electrophoresis image (Figure 5.1) shows that both H1 (73 nt) and H2 (72 nt) are between 35 bp and 50 bp and the slightly reduced mobility of H1 can be attributed to the dye modification. The hybridization of H1 to L1 and H2 to L2 can be confirmed by the reduced mobility. Besides, no intermolecular hybridization was induced in all concentrations tested. Hence, the designed DNA sequences were further employed for hybridization chain reaction.

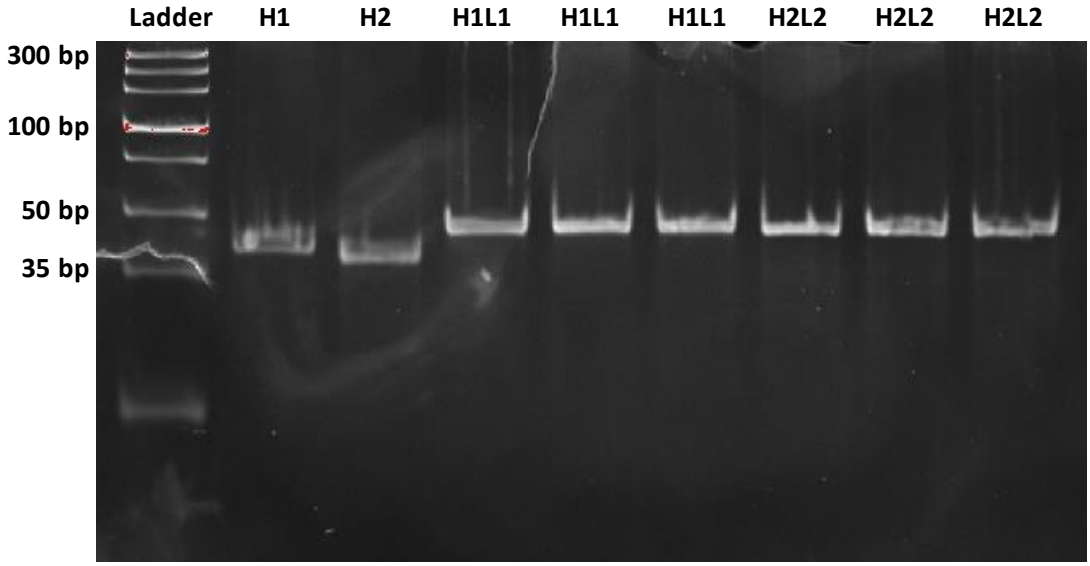

Figure 5.1. PAGE image of H1 and H2 prior to and after hybridization to ligand strands. H1 and H2 were prepared in 2 µM and H1L1 and H2L2 from left to right in 1 µM, 2 µM and 5 µM.

5.2 Hybridization chain reaction in solution

Next, successful hybridization chain reaction in solution was confirmed with gel electrophoresis and fluorescence measurements. As seen in Figure 5.2, no HCR was induced for DNA hairpins for either SiNP or AuNP in the absence of DNA initiator (band 6 in a and band 4 in b). When DNA initiator was introduced, however, clear HCR was initiated within 10 min, as evidenced by the sharp bands on top of the gels (band 7–9 in a and b). It was also found that the degree of polymerization is in inverse correlation with the amount of initiator as can be observed from the top bands of the gels (bands 7–9 in a and b).

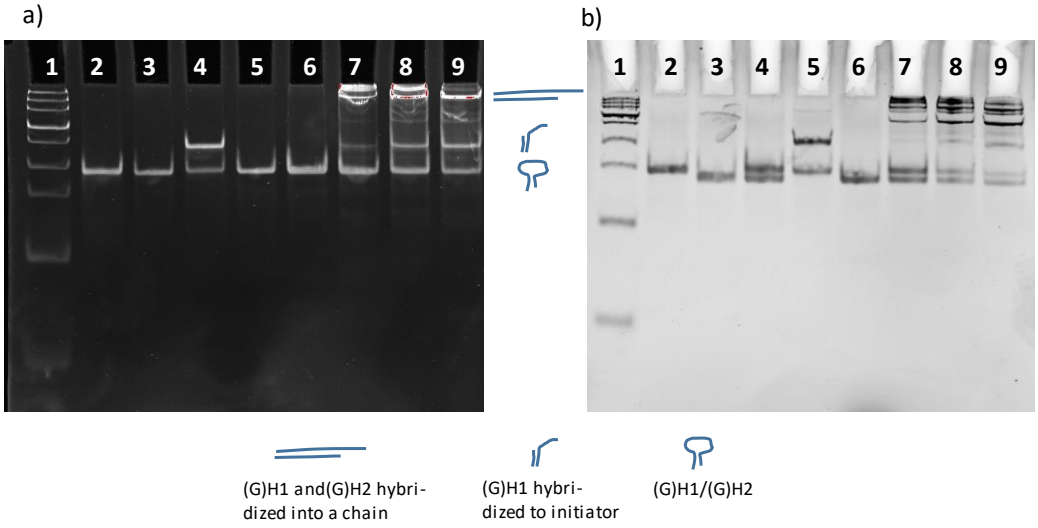

Figure 5.2. PAGE images of hybridization chain reaction test. a) DNAs for SiNPs: 1. Ladder 2. H1 3. H2 4. H1+I 5.H2+I 6. H1+H2 7. H1+H2+I (0.5×) 8. H1+H2+I (1×) 9. H1+H2+I (2×); b) DNAs for AuNPs: 1. Ladder 2. GH1 3. GH2 4. GH1+GH2 5.GH1+I 6. GH2+I 7. GH1+GH2+I (0.5×) 8. GH1+GH2+I (1×) 9. GH1+GH2+I (2×).

The HCR was also studied with time-dependent fluorescence measurement (Figure B.1 and Figure 5.3). It can be observed that the fluorescence intensity of H1 was dramatically quenched by L1 while no fluorescence signal was observed with H2 or H2L2 (Figure B.1). When the initiator was introduced, the fluorescence of H1 was partially recovered over the measurement period. Particularly, in the presence of

H2L2, faster and stronger fluorescence enhancement was observed and it increased with the amount of initiator added. This is predictable since in solution the HCR speed is highly dependent on the collision frequency, which is determined by the molecule concentration [10]. After confirming the successful HCR in solution, we sought to test it on NP surfaces.

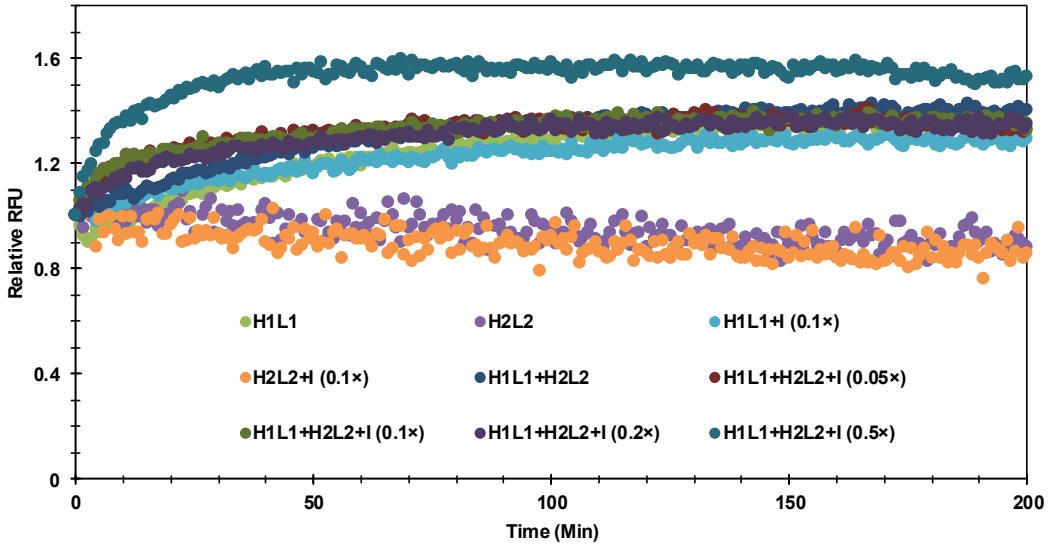

Figure 5.3. Time-dependent fluorescence of the hybridization chain reaction in PBS buffer.

5.3 Properties of silicon nanoparticles

For conjugating DNA hairpins to SiNPs, an efficient and selective thiol-maleimide reaction was used. Dynamic light scattering (DLS) was used to study and characterize the SiNPs before and after the maleimide modification. The diameter of the SiNPs was determined from intensity-based particle size distribution as an average of three measurements. The DLS measurement data in Figure 5.4a showed that the aminated SiNPs had aggregation caused by aqueous solution due to non-optimal pH. This caused the aminated SiNPs to have a wide size distribution. The maleimide-modified

SiNPs had a narrow size distribution of around 100 nm as expected and the increased particle size of maleimide-SiNPs can be attributed to the modification.

Successful maleimide modification was also verified by zeta potential measurements. As can be observed from Figure 5.4b, the zeta potential of bare SiNPs shifted from around 10 mV to -10 mV, confirming that the amine group has reacted with the cross-linker.

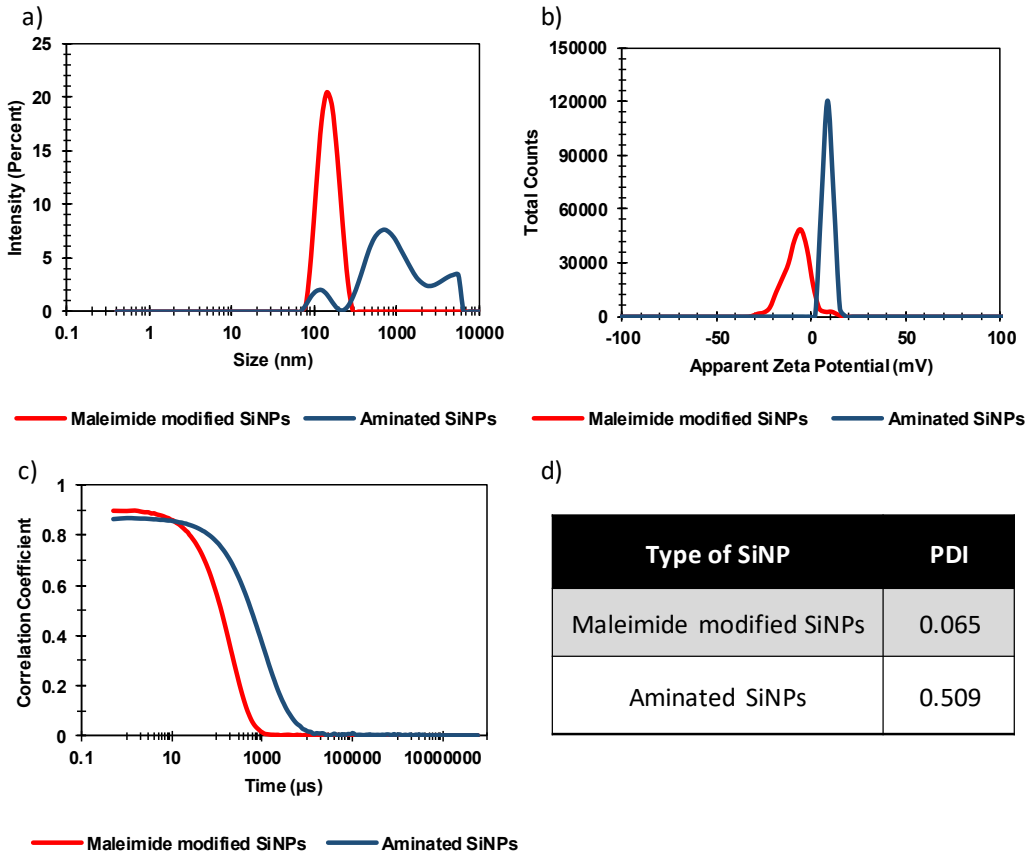

Type of SiNP	PDI
Maleimide modified SiNPs	0.065
Aminated SiNPs	0.509

Figure 5.4. a) The intensity-based size distribution of SiNPs and b) the zeta potentials of SiNPs before and after maleimide modification. c) The autocorrelation data and d) PDI values indicate that the maleimide modified SiNPs are monodisperse and aminated SiNPs have a wide size distribution.

5.4 DNA hairpin attachment to nanoparticles

The attachment of DNA to the nanoparticles (SiNPs and AuNPs) was determined by measuring the left-over DNA in the supernatant with UV/vis spectroscopy. During the study, parameters (temperature, reaction time and NaCl concentration) that can affect the DNA attachment to SiNPs were verified to optimize the conjugation condition.

As shown in Table 5.1, we found that both anchor DNAs, L1 and L2, showed similar attachment degree to SiNPs and the change in temperature or NaCl concentration didn't seem to affect the attachment of DNA hairpins to DNA anchors afterwards. Besides, the amount of excess DNA hairpins didn't affect the hybridization degree. The different attachment strategies are presented in Figure 5.5. When equal amounts of anchor DNAs was first combined and then attached to SiNPs, no subsequent hybridization of H1 and/or H2 were detected. When DNA anchors were first hybridized to corresponding DNA hairpins and followed by the conjugation, the conditions had more effect on the attachment. By increasing the NaCl concentration, the amount of attached DNAs rose a bit. Temperature and the longer attachment time had no obvious effect. The best result for the attachment was achieved by doing the reaction for 2 days at room temperature with 500 mM NaCl. Since H1/L1 and H2/L2 have similar attachment degrees respectively, we assumed that amount of H1/L1 and H2/L2 was the same. The obtained product was further used for the HCR evaluation in the next step. For the attachment of DNA hairpins to AuNPs, much higher degree was obtained, owing to the strong interaction between Au and thiol group on DNAs. The summary of the attachment for different type of DNAs to SiNPs can be seen in Table 5.1 and for AuNPs in Table 5.2. The calibration curves that were used to determine the amount of DNA in the supernatant in the UV/vis spectroscopy are presented in Appendix A.

Table 5.1. Typical attachment degrees for different types of DNAs to SiNPs. Attachment-% for L1, L2, H1L1 and H2L2 is the proportions attached from the added amount of DNA. For H1 and H2 the attachment-% means the percent of L1 and/or L2 is covered during the hybridization.

Type of DNA	Attachment-% (Mean±Std Dev)	Sample size	Confidence interval (Significance level 0.05)
L1	35±12	9	26-43
L2	37±9	9	32-42
H1	41±11	10	37-46
H2	45±9	27	41-48
H1L1	10±2	6	8-12
H2L2	9±2	10	8-10
H1L1 (2 days with 500 mM NaCl)	71	1	-
H2L2 (2 days with 500 mM NaCl)	70	1	-

Table 5.2. Typical attachment degrees for different types of DNAs to AuNPs. Attachment-% is the proportions attached from the added amount of DNA.

Type of DNA	Attachment-% (Mean±Std Dev)	Sample size	Confidence interval (Significance level 0.05)
GH1	45	1	-
GH2	47	1	-
GH1+GH2	48	1	-
Summary	47±2	3	45-49

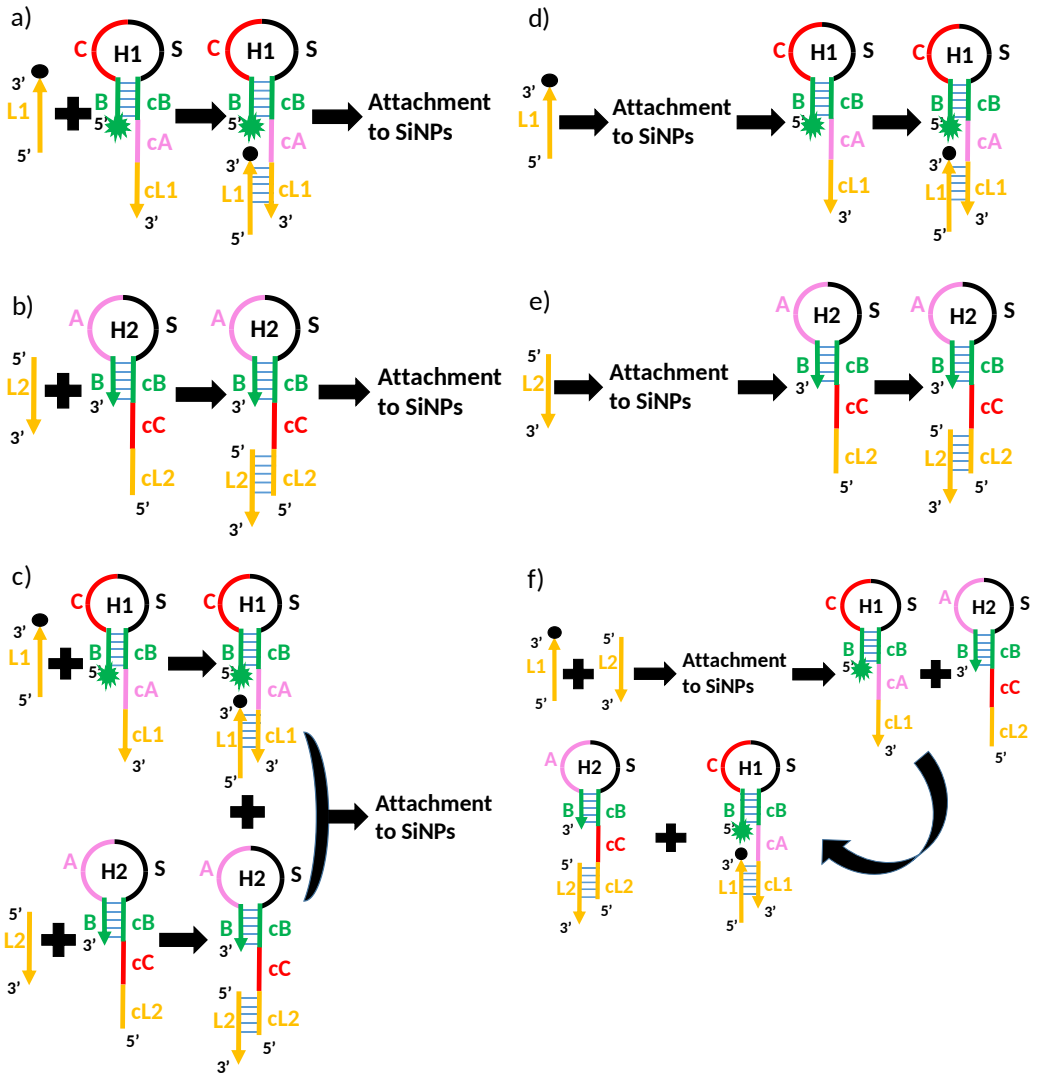

Figure 5.5. Coupling strategies used in the study. In the left a-c) are the strategies where the anchor DNAs were first hybridized to the corresponding stem-loop DNA and then attached to the SiNPs. On the right d-f) are the strategies where the anchor DNA was first attached to the SiNPs and then the corresponding stem-loop DNA were hybridized.

The presence of H2L2 DNA on SiNPs was also verified by TEM images. The stained DNA is clearly visible as a halo around the SiNPs in the TEM images (Figure 5.6) and the images also verify the uniform 100 nm size of the SiNPs. Only anchor DNA on top of the SiNPs could not be imaged due to its small size.

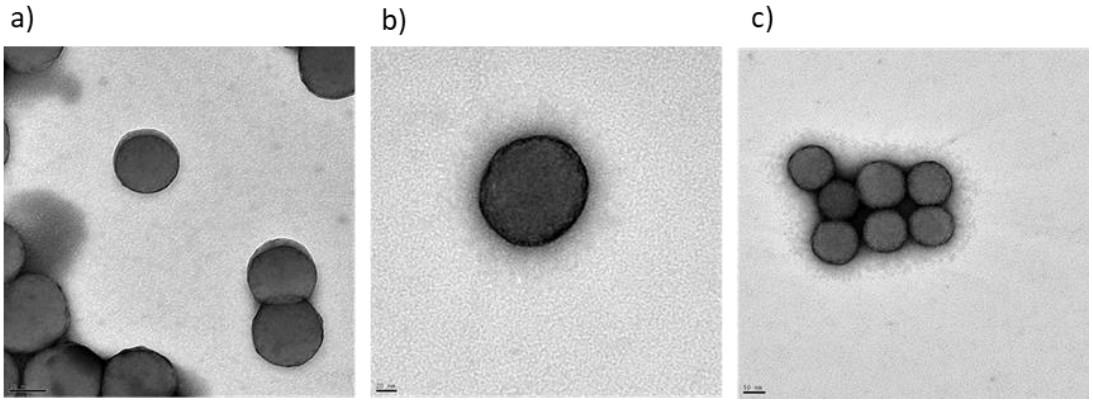

Figure 5.6. TEM images of SiNPs. a) SiNPs without DNA b) and c) SiNPs with both the anchor and hairpin loop DNAs on top of the nanoparticles. The DNA shell is seen as a halo around the SiNPs.

5.5 Hybridization chain reaction on top of nanoparticles

Time-dependent fluorescence measurement was used to test the hybridization chain reaction on the surface of the nanoparticles. In Figure 5.7, the fluorescence (excitation wavelength of 488 nm and the emission wavelength of 520 nm) of HCR in solution and on SiNPs over time was compared. In solution, H1L1 can hybridize with DNA initiator (10 mol% of H1L1), with or without H2L2, as evidenced by the fluorescence increase. On the other hand, SiNPs with H1L1 exhibited higher fluorescence comparing to that with H2L2, demonstrating the successful attachment of H1L1 (Figure B.2). However, the addition of initiator (10 mol% of H1L1) had no effect on the fluorescence intensity over the time period, which indicates that the H1L1 stem-loop was partially opened during the attachment reaction, as proven by the PAGE images (band 6, Figure 5.8).

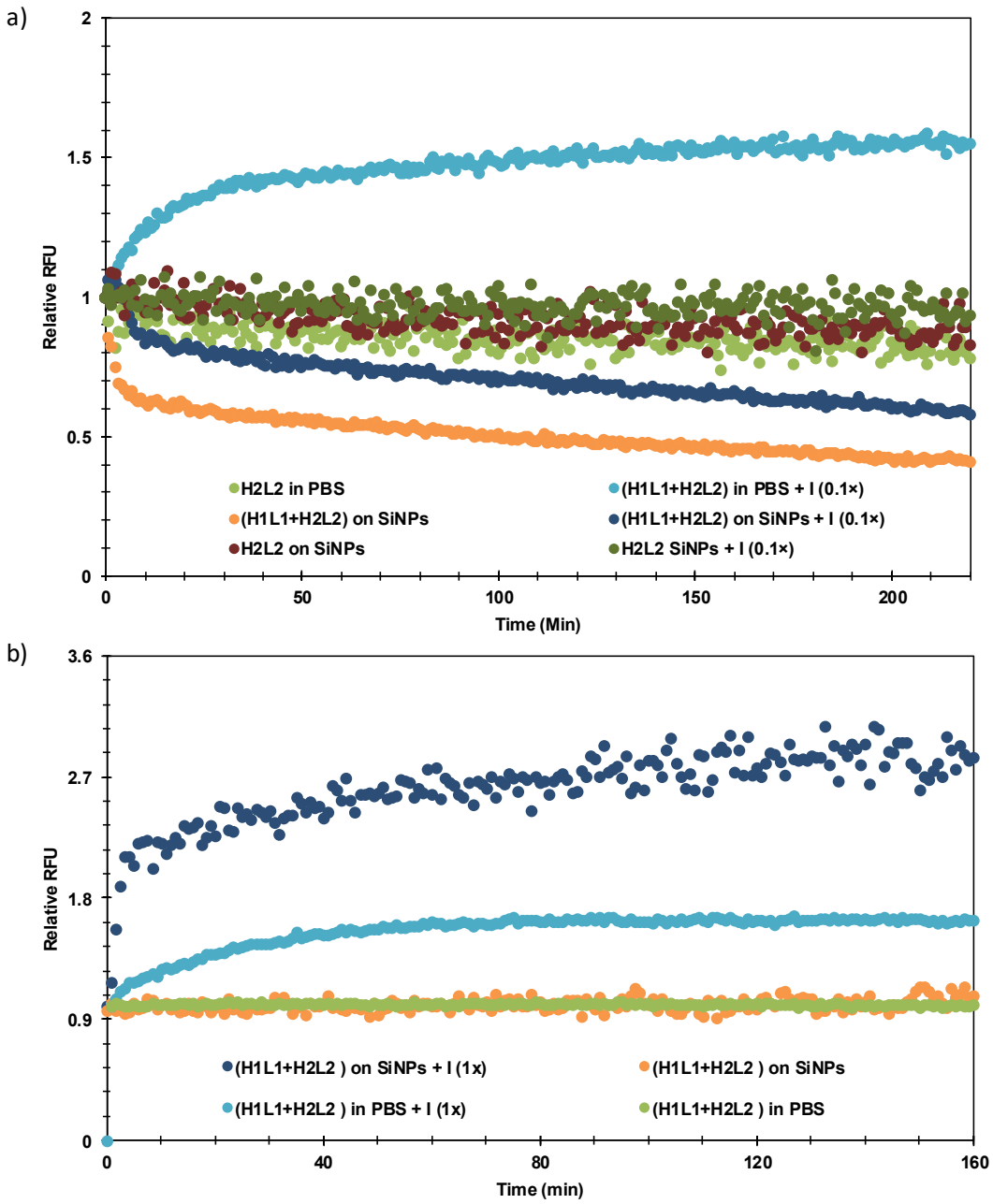

Figure 5.7. Relative time-dependent fluorescence of HCR on the surface of SiNPs. a) Relative RFU with 0.1× initiator. b) Relative RFU with 1× initiator.

Continuous fluorescence intensity decrease may be attributed to the quenching effect from the excitation, as can also be observed from H1 in solution (Figure B.2). Relatively low initiator concentration may also be one of the reason. When 1× DNA initiator was added, clear difference was observed between the HCR in solution and

on SiNPs. As can be seen in Figure 5.8b, the HCR speed and fluorescence increase are both higher than that initiated in solution, demonstrating the versatility of the SiNP-based HCR. However, optimization is still needed for ultralow RNA detection.

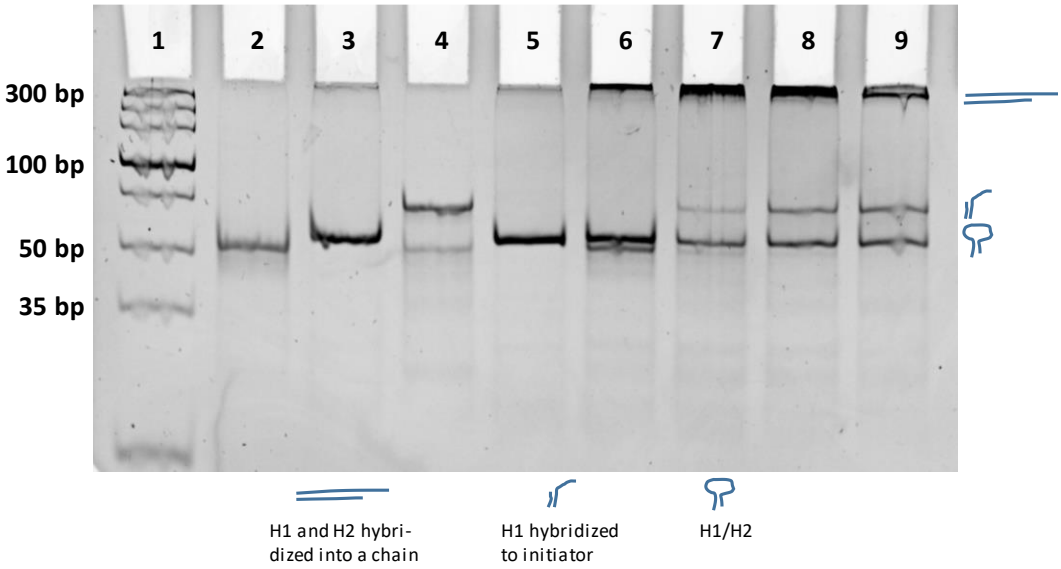

Figure 5.8. PAGE images of hybridization chain reaction test after overnight incubation of DNAs for SiNPs. 1. Ladder 2. H1 3. H2 4. H1+I 5.H2+I 6. H1+H2 (supernatant from the reaction) 7. H1+H2+I (0.5×) 8. H1+H2+I (1×) 9. H1+H2+I (2×).

Fluorescence test results obtained from AuNPs are presented in Figure 5.9. The fluorescence intensity of H1 conjugated to AuNPs was much lower than that of mixture of free H1 and AuNPs, demonstrating excellent quenching effect of AuNPs. When comparing that quenching effect between BHQ1 and AuNPs, the effect is similar (Figure B.3). The quenching effect of the AuNPs seems to be too strong that no clear fluorescence increase could be observed when initiator was introduced. This can be attributed to the relative big size of the AuNPs [118], leading to enormous quenching effect on FAM. Interaction between opened DNAs and AuNPs may also play a role in the phenomenon. The PAGE test (Figure 5.10) indicated that the DNA hairpins were stable and ring opening wasn't happening without initiator after overnight incubation, which would suggest that the H1 on top of the AuNPs would not open without the initiator. Hence, further optimization is needed for successful

HCR-induced fluorescence enhancement on AuNP and test on small size AuNP (5 nm) is on-going.

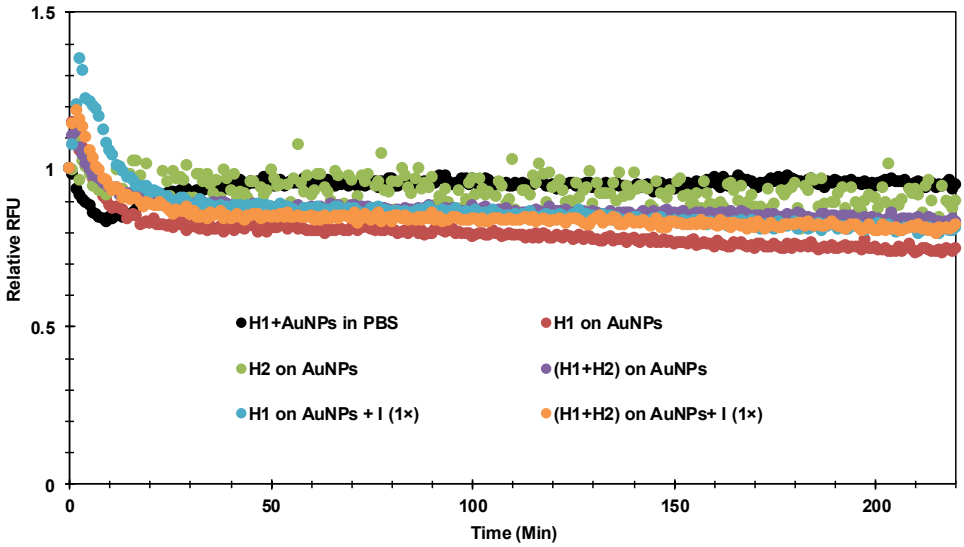

Figure 5.9. Relative time-dependent fluorescence of HCR on the surface of AuNPs.

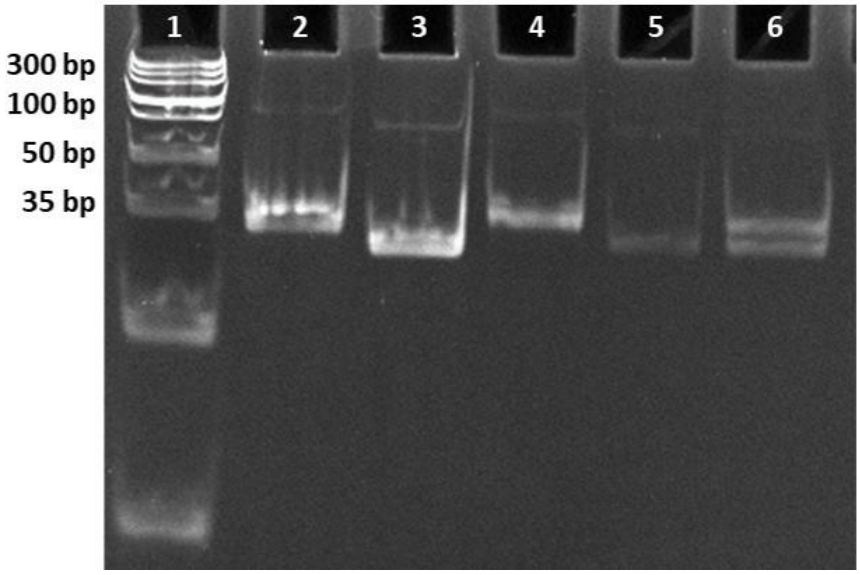

Figure 5.10. PAGE image of DNAs for gold nanoparticles after overnight incubation. 1. Ladder 2. H1 3. H2 4. H1 5. H2 6. H1+H2.

6. Conclusions and future perspectives

The results achieved in this thesis demonstrate a successful HCR in solution, as proved by PAGE and fluorescence spectra. Successful modification of SiNPs was also achieved, as proved by zeta potential measurement. The attachment degree of DNA on nanoparticles (SiNPs and AuNPs) was determined with UV/vis spectroscopy, which demonstrated a successful and predictable attachment to both NPs. The presence of H2L2 DNA on SiNPs was also verified by TEM images. The HCR on NPs was tested with time-dependent fluorescence spectra. The results demonstrated that SiNPs with H1L1 exhibited higher fluorescence compared to that with H2L2. However, addition of 0.1× DNA initiator had no effect on the fluorescence intensity suggesting that the H1L1 stem-loop was partially opened during the attachment reaction. When 1× DNA initiator was added, the HCR speed and fluorescence increase were both higher than that initiated in solution, demonstrating the versatility of the SiNP-based HCR. For AuNPs, the fluorescence intensity of H1 conjugated to AuNPs was much lower than that of mixture containing free H1 and AuNPs, demonstrating excellent quenching effect of AuNPs. The DNA hairpins on gold nanoparticles were stable but the quenching effect of the 10 nm AuNPs was too high to detect any differences in fluorescence intensity. This could be attributed to the relative big size of the AuNPs or interaction between opened DNAs and AuNPs.

To continue this study, changes in the DNA designs for SiNPs are necessary to prevent the ring opening from happening without initiator. For the gold nanoparticles, smaller AuNPs (5 nm) could be tested to evaluate if the quenching effect would mitigate. In principle, if the problems are solved, the method should lead to much faster detection speeds and higher detection sensitivity than those in non-constrained chain reactions.

References

[1] Sawyers CL. The cancer biomarker problem. Nature 2008;452(7187):548.

[2] Cohen C, Lohmann CM, Cotsonis G, Lawson D, Santoianni R. Survivin expression in ovarian carcinoma: correlation with apoptotic markers and prognosis. Modern pathology 2003;16(6):574.

[3] Kallio MJ, Nieminen M, Eriksson JE. Human inhibitor of apoptosis protein (IAP) survivin participates in regulation of chromosome segregation and mitotic exit. The FASEB Journal 2001;15(14):2721-2723.

[4] Cohen C, Lohmann CM, Cotsonis G, Lawson D, Santoianni R. Survivin expression in ovarian carcinoma: correlation with apoptotic markers and prognosis. Modern Pathology 2003;16(6):574.

[5] Fenstermaker RA, Figel SA, Qiu J, Barone TA, Dharma SS, Winograd EK, et al. Survivin monoclonal antibodies detect survivin cell surface expression and inhibit tumor growth in vivo. Clinical Cancer Research 2018;24(11):2642-2652.

[6] Dirks RM, Pierce NA. Triggered amplification by hybridization chain reaction. Proceedings of the National Academy of Sciences. 2004:101(43):15275-15278.

[7] Evanko D. Hybridization chain reaction. Nature Methods 2004;1(3):186.

[8] Wu Z, Liu G, Yang X, Jiang J. Electrostatic nucleic acid nanoassembly enables hybridization chain reaction in living cells for ultrasensitive mRNA imaging. Journal of the American Chemical Society 2015;137(21):6829-6836.

[9] Li L, Feng J, Liu H, Li Q, Tong L, Tang B. Two-color imaging of microRNA with enzyme-free signal amplification via hybridization chain reactions in living cells. Chemical Ccience 2016;7(3):1940-1945.

[10] Ren K, Xu Y, Liu Y, Yang M, Ju H. A responsive “nano string light” for highly efficient mRNA imaging in living cells via accelerated DNA cascade reaction. ACS Nano 2017;12(1):263-271.

[11] Bui H, Shah S, Mokhtar R, Song T, Garg S, Reif J. Localized DNA hybridization chain reactions on DNA origami. ACS Nano 2018;12(2):1146-1155.

[12] Mirkin CA, Letsinger RL, Mucic RC, Storhoff JJ. A DNA-based method for rationally assembling nanoparticles into macroscopic materials. Nature 1996;382(6592):607.

[13] Seeman NC, Sleiman HF. DNA nanotechnology. Nature Reviews Materials 2018;3(1):17068.

[14] Nelson DL, Lehninger AL, Cox MM. Lehninger principles of biochemistry, 4th ed. New York. Macmillan; 2008:1119.

[15] Alberts B, Johnson A, Lewis J, Morgan D, Raff M, Roberts K, et al. Molecular biology of the cell, 6th ed. New York. NY: WW Norton & Company 2014:1342.

[16] Kuriyan J, Konforti B, Wemmer D. The molecules of life: Physical and chemical principles, 4th ed. New York : Garland Science; 2012:1008.

[17] Lin C, Liu Y, Yan H. Designer DNA nanoarchitectures. Biochemistry (NY) 2009;48(8):1663-1674.

[18] Yakovchuk P, Protozanova E, Frank-Kamenetskii MD. Base-stacking and base-pairing contributions into thermal stability of the DNA double helix. Nucleic Acids Research 2006;34(2):564-574.

[19] Aldaye FA, Palmer AL, Sleiman HF. Assembling materials with DNA as the guide. Science 2008;321(5897):1795-1799.

[20] Watson JD, Crick FH. Molecular structure of nucleic acids; a structure for deoxyribose nucleic acid. Nature 1953;171(4356):737-738.

[21] Berg J, Tymoczko J, Stryer L. Biochemistry, 7th ed. New York: W. H. Freeman and Company; 2012:1098.

[22] Yang D, Campolongo MJ, Nhi Tran TN, Ruiz RC, Kahn JS, Luo D. Novel DNA materials and their applications. Wiley Interdisciplinary Reviews: Nanomedicine and Nanobiotechnology 2010;2(6):648-669.

[23] Blackburn GM, Gait MJ, Loakes D, Williams DM. Nucleic acids in chemistry and biology, 3rd ed. Oxford: The Royal Society of Chemistry; 2006. p. 470.

[24] Liedl T, Sobey TL, Simmel FC. DNA-based nanodevices. Nano Today 2007;2(2):36-41.

[25] Zhang F, Nangreave J, Liu Y, Yan H. Structural DNA nanotechnology: state of the art and future perspective. Journal of the American Chemical Society 2014;136(32):11198-11211.

[26] Bath J, Turberfield A. DNA nanomachines. Nature.Nanotechnology 2007;2:275-284.

[27] Modi S, Bhatia D, Simmel FC, Krishnan Y. Structural DNA nanotechnology: from bases to bricks, from structure to function. The Journal of Physical Chemistry Letters 2010;1(13):1994-2005.

[28] He Y, Chen Y, Liu H, Ribbe AE, Mao C. Self-assembly of hexagonal DNA two-dimensional (2D) arrays. Journal of the American Chemical Society 2005;127(35):12202-12203.

[29] Yurke B, Turberfield AJ, Mills Jr AP, Simmel FC, Neumann JL. A DNA-fuelled molecular machine made of DNA. Nature 2000;406(6796):605.

[30] English DS, Pell LE, Yu Z, Barbara PF, Korgel BA. Size tunable visible luminescence from individual organic monolayer stabilized silicon nanocrystal quantum dots. Nano Letters 2002;2(7):681-685.

[31] Rosso-Vasic M, Spruijt E, Popović Z, Overgaag K, Van Lagen B, Grandidier B, et al. Amine-terminated silicon nanoparticles: synthesis, optical properties and their use in bioimaging. Journal of Materials Chemistry 2009;19(33):5926-5933.

[32] Delerue C, Allan G, Lannoo M. Theoretical aspects of the luminescence of porous silicon. Physical Review B 1993;48(15):11024.

[33] Zou J, Baldwin RK, Pettigrew KA, Kauzlarich SM. Solution synthesis of ultrastable luminescent siloxane-coated silicon nanoparticles. Nano Letters 2004;4(7):1181-1186.

[34] Veinot JG. Synthesis, surface functionalization, and properties of freestanding silicon nanocrystals. Chemical Communications 2006(40):4160-4168.

[35] Evlyukhin AB, Reinhardt C, Chichkov BN. Multipole light scattering by nonspherical nanoparticles in the discrete dipole approximation. Physical Review B 2011;84(23):235429.

[36] Garcia-Etxarri A, Gómez-Medina R, Froufe-Perez LS, Lopez C, Chantada L, Scheffold F, et al. Strong magnetic response of submicron silicon particles in the infrared. Optics Express 2011;19(6):4815-4826.

[37] Evlyukhin AB, Reinhardt C, Seidel A, Luk'yanchuk BS, Chichkov BN. Optical response features of Si-nanoparticle arrays. Physical Review B 2010;82(4):045404.

[38] Evlyukhin A, Kuznetsov A, Novikov S, Beermann J, Reinhardt C, Kiyan R, et al. Optical properties of spherical gold mesoparticles. Applied Physics B 2012;106(4):841-848.

[39] Kuznetsov AI, Miroshnichenko AE, Fu YH, Zhang J, Luk'Yanchuk B. Magnetic light. Scientific Reports 2012;2:492.

[40] Hua F, Erogbogbo F, Swihart MT, Ruckenstein E. Organically capped silicon nanoparticles with blue photoluminescence prepared by hydrosilylation followed by oxidation. Langmuir 2006;22(9):4363-4370.

[41] Li X, He Y, Swihart MT. Surface functionalization of silicon nanoparticles produced by laser-driven pyrolysis of silane followed by HF− HNO3 etching. Langmuir 2004;20(11):4720-4727.

[42] Heinrich JL, Curtis CL, Credo GM, Sailor MJ, Kavanagh KL. Luminescent colloidal silicon suspensions from porous silicon. Science 1992:255(5040):66-68.

[43] Mangolini L, Thimsen E, Kortshagen U. High-yield plasma synthesis of luminescent silicon nanocrystals. Nano letters 2005;5(4):655-659.

[44] Wilcoxon J, Samara G. Tailorable, visible light emission from silicon nanocrystals. Applied Physics Letters 1999;74(21):3164-3166.

[45] English DS, Pell LE, Yu Z, Barbara PF, Korgel BA. Size tunable visible luminescence from individual organic monolayer stabilized silicon nanocrystal quantum dots. Nano Letters 2002;2(7):681-685.

[46] Holmes JD, Ziegler KJ, Doty RC, Pell LE, Johnston KP, Korgel BA. Highly luminescent silicon nanocrystals with discrete optical transitions. Journal of the American Chemical Society 2001;123(16):3743-3748.

[47] Pettigrew KA, Liu Q, Power PP, Kauzlarich SM. Solution synthesis of alkyl-and alkyl/alkoxy-capped silicon nanoparticles via oxidation of Mg_2Si. Chemistry of Materials 2003;15(21):4005-4011.

[48] Neiner D, Chiu HW, Kauzlarich SM. Low-temperature solution route to macroscopic amounts of hydrogen terminated silicon nanoparticles. Journal of the American Chemical Society 2006;128(34):11016-11017.

[49] Rosso-Vasic M, Spruijt E, van Lagen B, De Cola L, Zuilhof H. Alkyl-Functionalized Oxide-Free Silicon Nanoparticles: Synthesis and Optical Properties. Small 2008;4(10):1835-1841.

[50] Tilley RD, Warner JH, Yamamoto K, Matsui I, Fujimori H. Micro-emulsion synthesis of monodisperse surface stabilized silicon nanocrystals. Chemical Communications 2005(14):1833-1835.

[51] Wilson WL, Szajowski PF, Brus LE. Quantum confinement in size-selected, surface-oxidized silicon nanocrystals. Science 1993:262(5137):1242-1244.

[52] Wang L, Reipa V, Blasic J. Silicon nanoparticles as a luminescent label to DNA. Bioconjugate Chemistry 2004;15(2):409-412.

[53] Li Z, Ruckenstein E. Water-soluble poly (acrylic acid) grafted luminescent silicon nanoparticles and their use as fluorescent biological staining labels. Nano Letters 2004;4(8):1463-1467.

[54] Wang J, Ye D, Liang G, Chang J, Kong J, Chen J. One-step synthesis of water-dispersible silicon nanoparticles and their use in fluorescence lifetime imaging of living cells. Journal of Materials Chemistry B 2014;2(27):4338-4345.

[55] Popplewell J, King S, Day J, Ackrill P, Fifield L, Cresswell R, et al. Kinetics of uptake and elimination of silicic acid by a human subject: a novel application of 32Si and accelerator mass spectrometry. Journal of Inorganic Biochemistry 1998;69(3):177-180.

[56] Salonen J, Kaukonen AM, Hirvonen J, Lehto V. Mesoporous silicon in drug delivery applications. Journal of Pharmaceutical Sciences 2008;97(2):632-653.

[57] Daniel M, Astruc D. Gold nanoparticles: assembly, supramolecular chemistry, quantum-size-related properties, and applications toward biology, catalysis, and nanotechnology. Chemical Reviews 2004;104(1):293-346.

[58] Ghosh SK, Pal T. Interparticle coupling effect on the surface plasmon resonance of gold nanoparticles: from theory to applications. Chemical Reviews 2007;107(11):4797-4862.

[59] Zeng S, Yong K, Roy I, Dinh X, Yu X, Luan F. A review on functionalized gold nanoparticles for biosensing applications. Plasmonics 2011;6(3):491.

[60] Eustis S, El-Sayed MA. Why gold nanoparticles are more precious than pretty gold: noble metal surface plasmon resonance and its enhancement of the radiative and nonradiative properties of nanocrystals of different shapes. Chemical Society Reviews 2006;35(3):209-217.

[61] Zhao W, Brook MA, Li Y. Design of gold nanoparticle-based colorimetric biosensing assays. ChemBioChem 2008;9(15):2363-2371.

[62] Shipway AN, Lahav M, Gabai R, Willner I. Investigations into the electrostatically induced aggregation of Au nanoparticles. Langmuir 2000;16(23):8789-8795.

[63] Mie G. Beiträge zur Optik trüber Medien, speziell kolloidaler Metallösungen. Annalen der Physik 1908;330(3):377-445.

[64] Willets KA, Van Duyne RP. Localized surface plasmon resonance spectroscopy and sensing. The Annual Review of Physical Chemistry 2007;58:267-297.

[65] Grzelczak M, Pérez-Juste J, Mulvaney P, Liz-Marzán LM. Shape control in gold nanoparticle synthesis. Chemical Society Reviews 2008;37(9):1783-1791.

[66] Giljohann DA, Seferos DS, Daniel WL, Massich MD, Patel PC, Mirkin CA. Gold nanoparticles for biology and medicine. Angewandte Chemie International Edition 2010;49(19):3280-3294.

[67] Dreaden EC, Alkilany AM, Huang X, Murphy CJ, El-Sayed MA. The golden age: gold nanoparticles for biomedicine. Chemical Society Reviews 2012;41(7):2740-2779.

[68] Zhao P, Li N, Astruc D. State of the art in gold nanoparticle synthesis. Coordination Chemistry Reviews 2013;257(3-4):638-665.

[69] Samanta A, Banerjee S, Liu Y. DNA nanotechnology for nanophotonic applications. Nanoscale 2015;7(6):2210-2220.

[70] Shipway AN, Katz E, Willner I. Nanoparticle arrays on surfaces for electronic, optical, and sensor applications. ChemPhysChem 2000;1(1):18-52.

[71] Rosi NL, Mirkin CA. Nanostructures in biodiagnostics. Chemical Reviews 2005;105(4):1547-1562.

[72] Ghosh P, Han G, De M, Kim CK, Rotello VM. Gold nanoparticles in delivery applications. Advanced Drug Delivery Reviews 2008;60(11):1307-1315.

[73] Lohse SE, Murphy CJ. Applications of colloidal inorganic nanoparticles: from medicine to energy. Journal of the American Chemical Society 2012;134(38):15607-15620.

[74] Ofir Y, Samanta B, Rotello VM. Polymer and biopolymer mediated self-assembly of gold nanoparticles. Chemical Society Reviews 2008;37(9):1814-1825.

[75] Nie Z, Petukhova A, Kumacheva E. Properties and emerging applications of self-assembled structures made from inorganic nanoparticles. Nature nanotechnology 2010;5(1):15.

[76] Giljohann DA, Seferos DS, Daniel WL, Massich MD, Patel PC, Mirkin CA. Gold nanoparticles for biology and medicine. Angewandte Chemie International Edition 2010;49(19):3280-3294.

[77] Rosi NL, Giljohann DA, Thaxton CS, Lytton-Jean AK, Han MS, Mirkin CA. Oligonucleotide-modified gold nanoparticles for intracellular gene regulation. Science 2006:312(5776):1027-1030.

[78] Bruchez M,Jr, Moronne M, Gin P, Weiss S, Alivisatos AP. Semiconductor nanocrystals as fluorescent biological labels. Science 1998;281(5385):2013-2016.

[79] Farokhzad OC, Langer R. Nanomedicine: developing smarter therapeutic and diagnostic modalities. Advanced Drug Delivery Reviews 2006;58(14):1456-1459.

[80] Seferos DS, Giljohann DA, Hill HD, Prigodich AE, Mirkin CA. Nano-flares: probes for transfection and mRNA detection in living cells. Journal of the American Chemical Society 2007;129(50):15477-15479.

[81] Kyriacou SV, Brownlow WJ, Xu XN. Using nanoparticle optics assay for direct observation of the function of antimicrobial agents in single live bacterial cells. Biochemistry (NY) 2004;43(1):140-147.

[82] Von Maltzahn G, Park J, Lin KY, Singh N, Schwöppe C, Mesters R, et al. Nanoparticles that communicate in vivo to amplify tumour targeting. Nature Materials 2011;10(7):545.

[83] Giljohann DA, Seferos DS, Prigodich AE, Patel PC, Mirkin CA. Gene regulation with polyvalent siRNA− nanoparticle conjugates. Journal of the American Chemical Society 2009;131(6):2072-2073.

[84] Cutler JI, Auyeung E, Mirkin CA. Spherical nucleic acids. Journal of the American Chemical Society 2012;134(3):1376-1391.

[85] Han D, Pal S, Nangreave J, Deng Z, Liu Y, Yan H. DNA origami with complex curvatures in three-dimensional space. Science 2011;332(6027):342-346.

[86] Seeman NC. DNA engineering and its application to nanotechnology. Trends in Biotechnology 1999;17(11):437-443.

[87] Seeman NC. DNA in a material world. Nature 2003;421(6921):427.

[88] Li Z, Jin R, Mirkin CA, Letsinger RL. Multiple thiol-anchor capped DNA–gold nanoparticle conjugates. Nucleic Acids Research 2002;30(7):1558-1562.

[89] Sato K, Hosokawa K, Maeda M. Rapid aggregation of gold nanoparticles induced by non-cross-linking DNA hybridization. Journal of the American Chemical Society 2003;125(27):8102-8103.

[90] Lee J, Lytton-Jean AK, Hurst SJ, Mirkin CA. Silver nanoparticle–oligonucleotide conjugates based on DNA with triple cyclic disulfide moieties. Nano Letters 2007;7(7):2112-2115.

[91] Cutler JI, Zheng D, Xu X, Giljohann DA, Mirkin CA. Polyvalent oligonucleotide iron oxide nanoparticle "click" conjugates. Nano Letters 2010;10(4):1477-1480.

[92] Mitchell GP, Mirkin CA, Letsinger RL. Programmed assembly of DNA functionalized quantum dots. Journal of the American Chemical Society 1999;121(35):8122-8123.

[93] Frens G. Controlled nucleation for the regulation of the particle size in monodisperse gold suspensions. Nature Physical Science 1973;241(105):20.

[94] Yin Y, Li Z, Zhong Z, Gates B, Xia Y, Venkateswaran S. Synthesis and characterization of stable aqueous dispersions of silver nanoparticles through the Tollens process. Journal of Materials Chemistry 2002;12(3):522-527.

[95] Ghosh SS, Kao PM, McCue AW, Chappelle HL. Use of maleimide-thiol coupling chemistry for efficient syntheses of oligonucleotide-enzyme conjugate hybridization probes. Bioconjugate Chemistry 1990;1(1):71-76.

[96] He D, He X, Wang K, Cao J, Zhao Y. A Photon-Fueled Gate-Like Delivery System Using i-Motif DNA Functionalized Mesoporous Silica Nanoparticles. Advanced Functional Materials 2012;22(22):4704-4710.

[97] Rosi NL, Mirkin CA. Nanostructures in biodiagnostics. Chemical Reviews 2005;105(4):1547-1562.

[98] Cutler JI, Zhang K, Zheng D, Auyeung E, Prigodich AE, Mirkin CA. Polyvalent nucleic acid nanostructures. Journal of the American Chemical Society 2011;133(24):9254-9257.

[99] Ren K, Xu Y, Liu Y, Yang M, Ju H. A responsive "nano string light" for highly efficient mRNA imaging in living cells via accelerated DNA cascade reaction. ACS Nano 2017;12(1):263-271.

[100] Zhao Y, Chen F, Li Q, Wang L, Fan C. Isothermal amplification of nucleic acids. Chemical Reviews 2015;115(22):12491-12545.

[101] Deng R, Tang L, Tian Q, Wang Y, Lin L, Li J. Toehold-initiated rolling circle amplification for visualizing individual microRNAs in situ in single cells. Angewandte Chemie International Edition 2014;53(9):2389-2393.

[102] Wu C, Cansiz S, Zhang L, Teng I, Qiu L, Li J, et al. A nonenzymatic hairpin DNA cascade reaction provides high signal gain of mRNA imaging inside live cells. Journal of the American Chemical Society 2015;137(15):4900-4903.

[103] Koos B, Cane G, Grannas K, Löf L, Arngården L, Heldin J, et al. Proximity-dependent initiation of hybridization chain reaction. Nature Communications 2015;6:7294.

[104] Li B, Jiang Y, Chen X, Ellington AD. Probing spatial organization of DNA strands using enzyme-free hairpin assembly circuits. Journal of the American Chemical Society 2012;134(34):13918-13921.

[105] Choi HM, Beck VA, Pierce NA. Next-generation in situ hybridization chain reaction: higher gain, lower cost, greater durability. ACS Nano 2014;8(5):4284-4294.

[106] Wang F, Lu C, Willner I. From cascaded catalytic nucleic acids to enzyme–DNA nanostructures: controlling reactivity, sensing, logic operations, and assembly of complex structures. Chemical Reviews 2014;114(5):2881-2941.

[107] Yin P, Choi HM, Calvert CR, Pierce NA. Programming biomolecular self-assembly pathways. Nature 2008;451(7176):318.

[108] Choi HM, Chang JY, Trinh LA, Padilla JE, Fraser SE, Pierce NA. Programmable in situ amplification for multiplexed imaging of mRNA expression. Nature Biotechnology 2010;28(11):1208.

[109] Choi J, Routenberg Love K, Gong Y, Gierahn TM, Love JC. Immuno-hybridization chain reaction for enhancing detection of individual cytokine-secreting human peripheral mononuclear cells. Analytical Chemistry 2011;83(17):6890-6895.

[110] Dalchau N, Chandran H, Gopalkrishnan N, Phillips A, Reif J. Probabilistic analysis of localized DNA hybridization circuits. ACS Synthetic Biology 2015;4(8):898-913.

[111] Muscat RA, Strauss K, Ceze L, Seelig G. DNA-based molecular architecture with spatially localized components. ACM SIGARCH Computer Architecture News: ACM; 2013: 41(3):177-88.

[112] Chandran H, Gopalkrishnan N, Phillips A, Reif J. Localized hybridization circuits. International Workshop on DNA-Based Computers: Springer; 2011:9:64-83.

[113] Ke G, Liu M, Jiang S, Qi X, Yang YR, Wootten S, et al. Directional regulation of enzyme pathways through the control of substrate channeling on a DNA origami scaffold. Angewandte Chemie International Edition 2016;55(26):7483-7486.

[114] Zhao Z, Fu J, Dhakal S, Johnson-Buck A, Liu M, Zhang T, et al. Nanocaged enzymes with enhanced catalytic activity and increased stability against protease digestion. Nature Communications 2016;7:10619.

[115] Lee JW, Na D, Park JM, Lee J, Choi S, Lee SY. Systems metabolic engineering of microorganisms for natural and non-natural chemicals. Nature Chemical Biology 2012;8(6):536.

[116] Agapakis CM, Boyle PM, Silver PA. Natural strategies for the spatial optimization of metabolism in synthetic biology. Nature Chemical Biology 2012;8(6):527.

[117] Wilson K, Walker J. Principles and techniques of biochemistry and molecular biology. : Cambridge University Press; 2010.

[118] Acuna GP, Bucher M, Stein IH, Steinhauer C, Kuzyk A, Holzmeister P, et al. Distance dependence of single-fluorophore quenching by gold nanoparticles studied on DNA origami. ACS Nano 2012;6(4):3189-3195.

[119] Khlebtsov BN, Khanadeev VA, Khlebtsov NG. Determination of the size, concentration, and refractive index of silica nanoparticles from turbidity spectra. Langmuir 2008;24(16):8964-8970.

[120] Ijäs H, Hakaste I, Shen B, Kostiainen MA, Linko V. Reconfigurable DNA Origami Nanocapsule for pH-Controlled Encapsulation and Display of Cargo. ACS Nano 2019.

[121] Castro CE, Kilchherr F, Kim D, Shiao EL, Wauer T, Wortmann P, et al. A primer to scaffolded DNA origami. Nature Methods 2011;8(3):221.

APPENDICES

Appendix A. Calibration curves using UV/Vis spectroscopy.

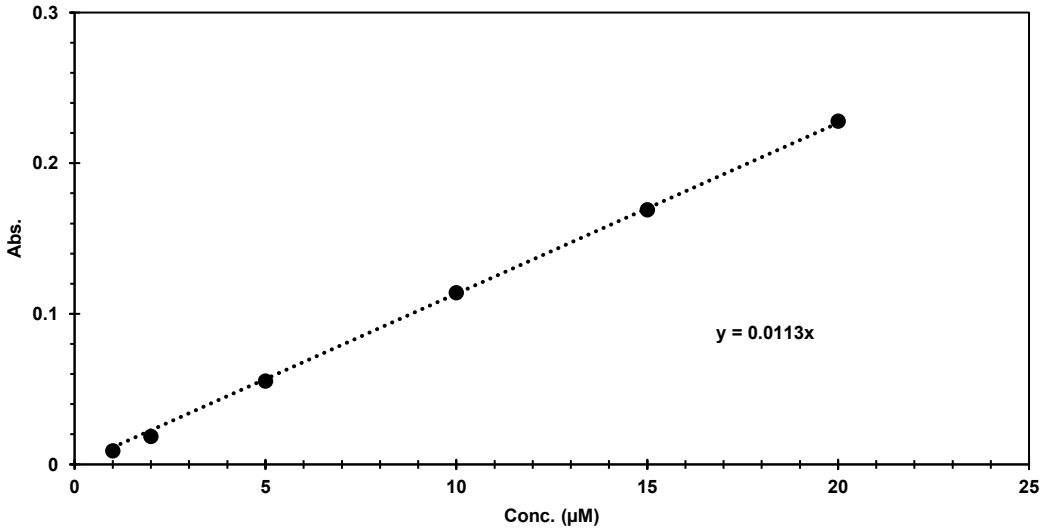

Figure A.1. Calibration curve for L1 DNA for silicon nanoparticles.

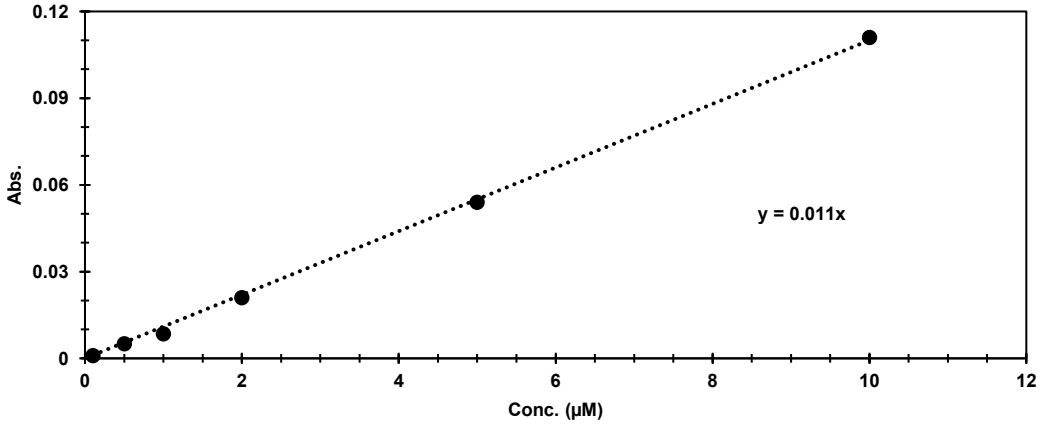

Figure A.2. Calibration curve for L2 DNA for silicon nanoparticles.

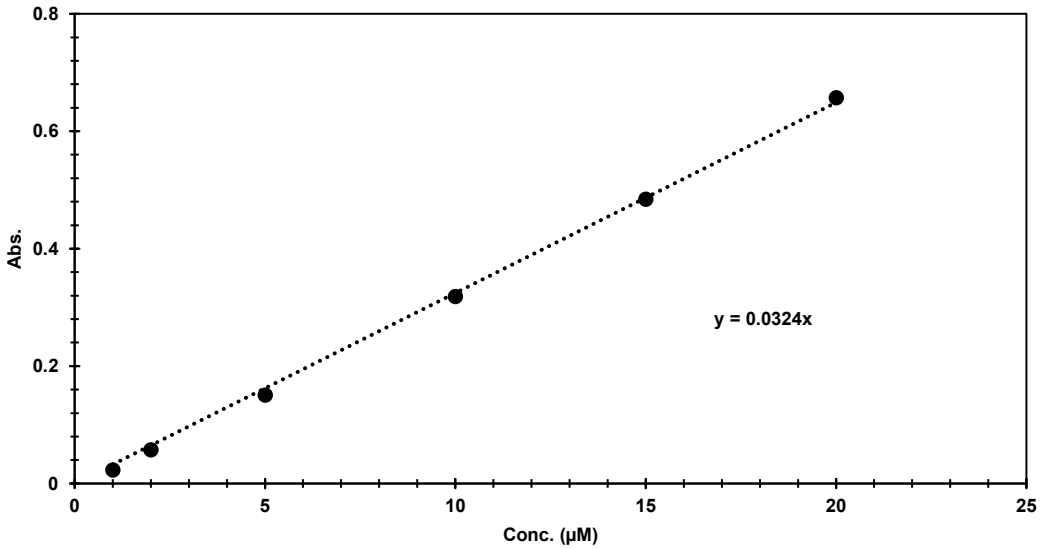

Figure A.3. Calibration curve for H1 DNA for silicon nanoparticles.

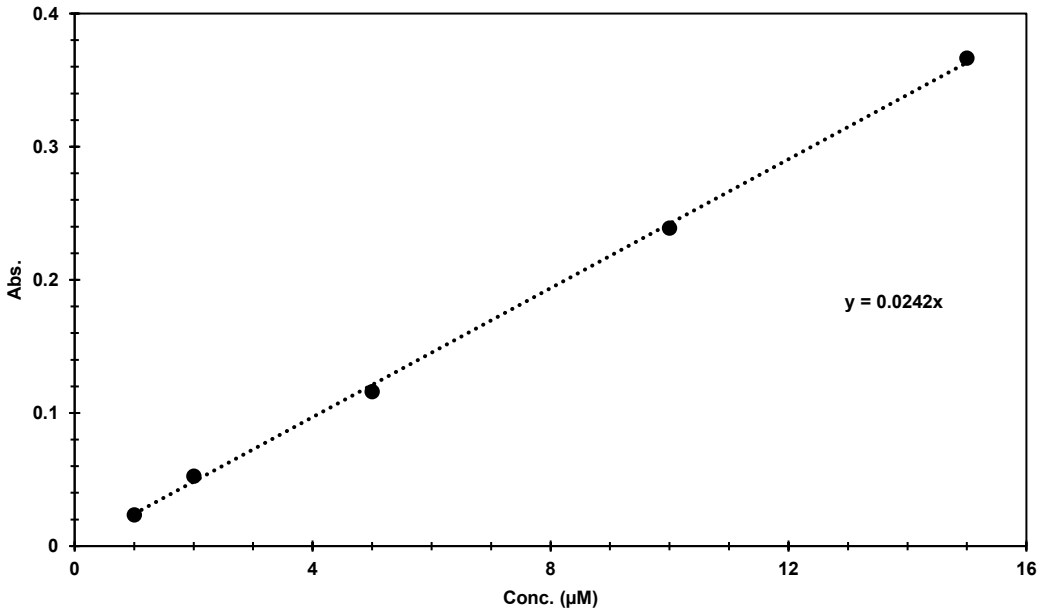

Figure A.4. Calibration curve for H2 DNA for silicon nanoparticles.

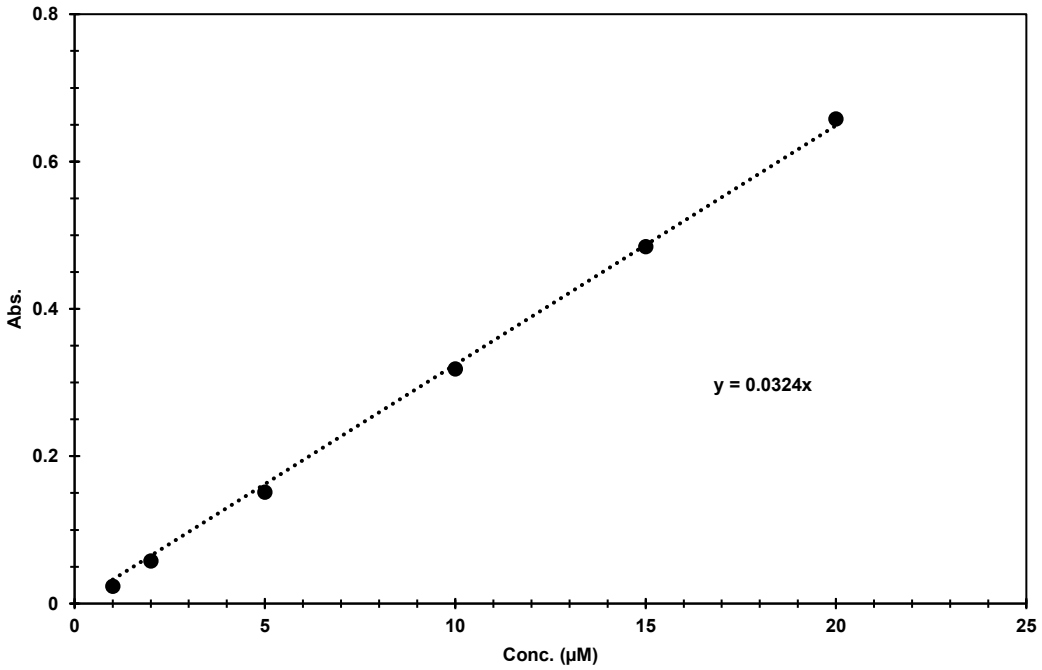

Figure A.5. Calibration curve for H1L1 DNA for silicon nanoparticles.

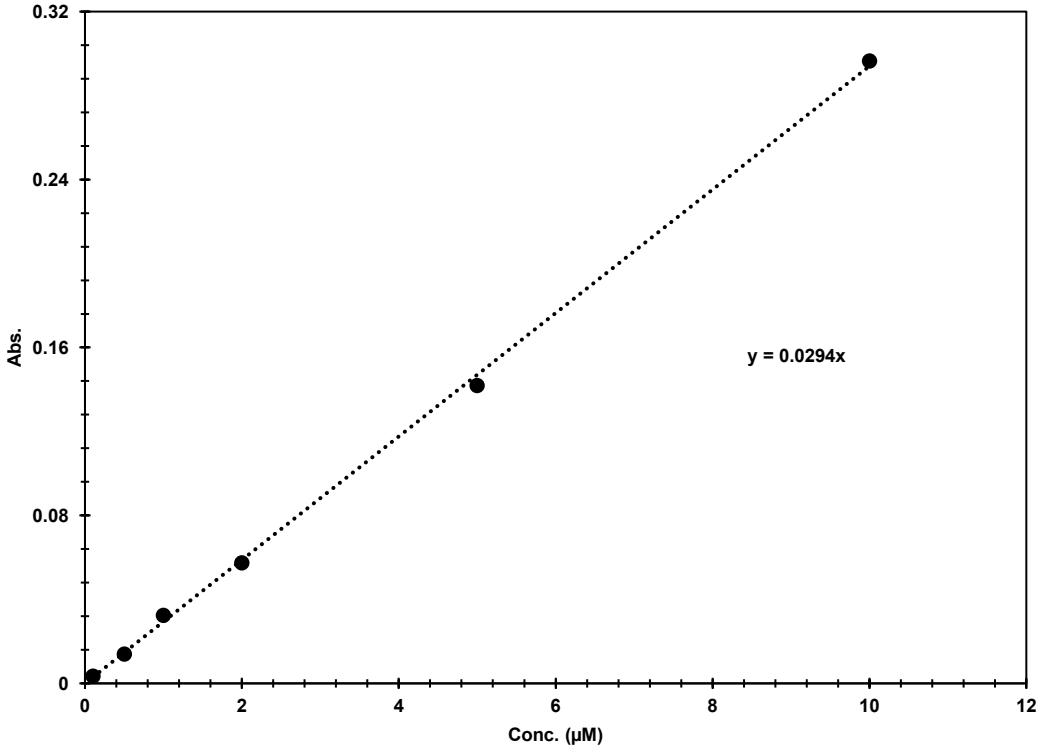

Figure A.6. Calibration curve for H2L2 DNA for silicon nanoparticles.

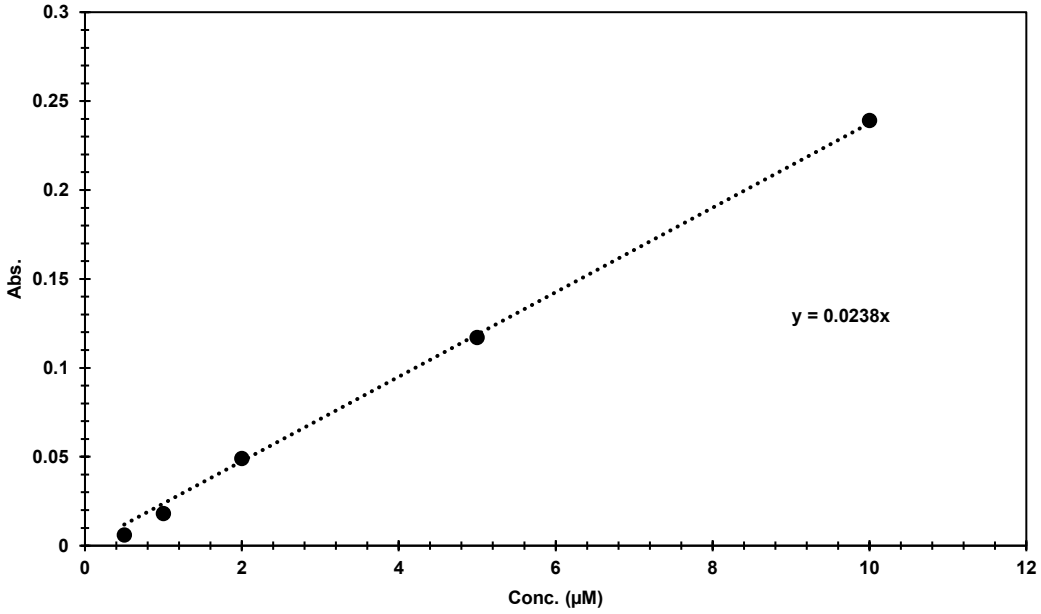

Figure A.7. Calibration curve for GH1 DNA for gold nanoparticles.

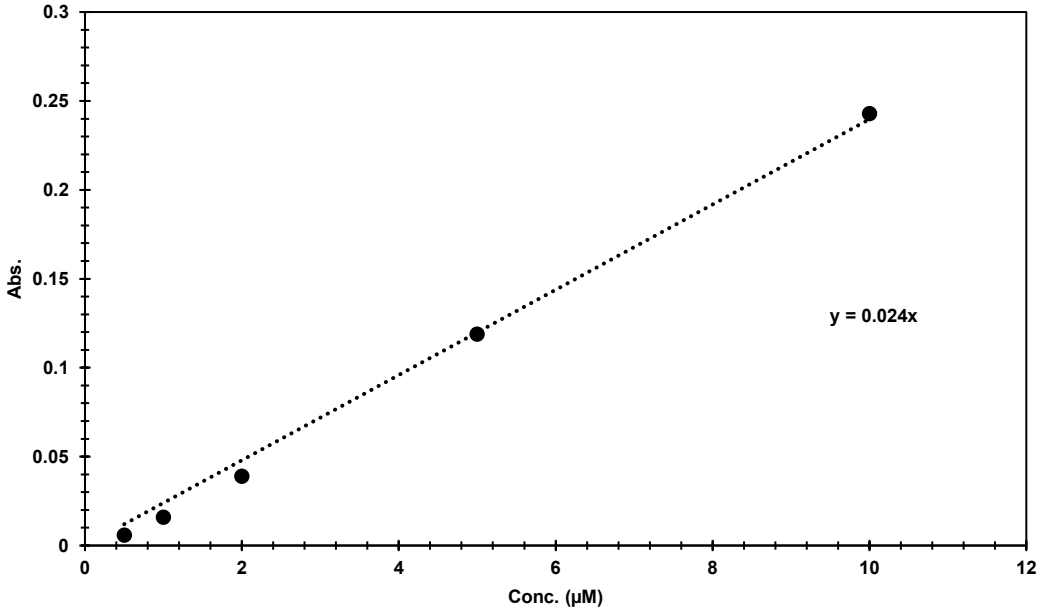

Figure A.8. Calibration curve for GH2 DNA for gold nanoparticles.

Appendix B. Time-dependent fluorescence spectras.

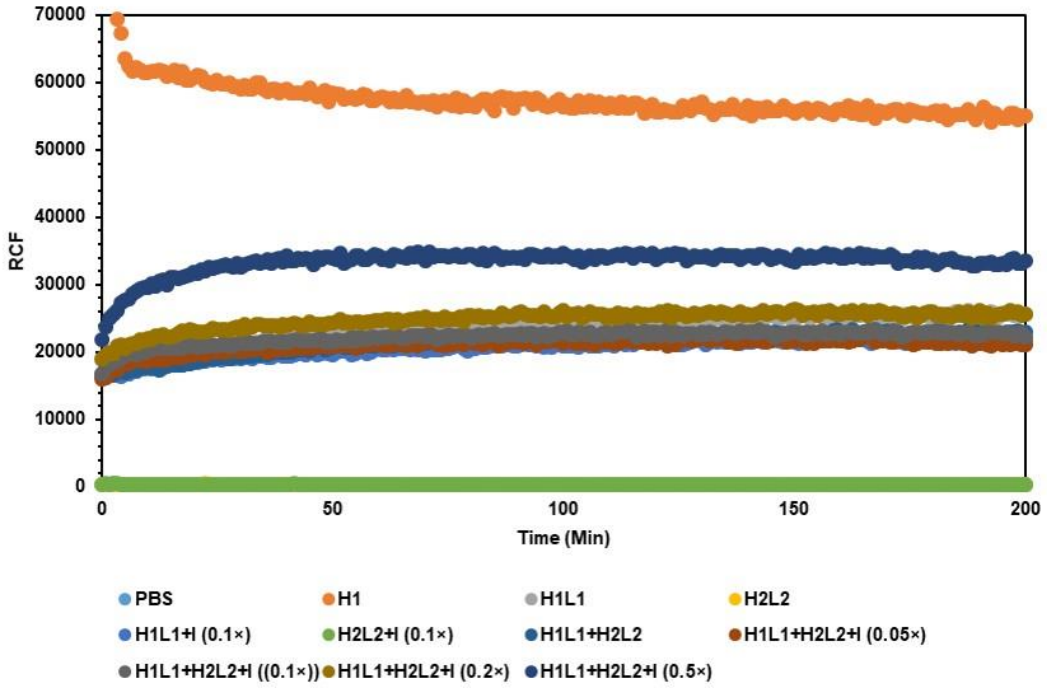

Figure B.1. Time-dependent fluorescence of the hybridization chain reaction in PBS buffer.

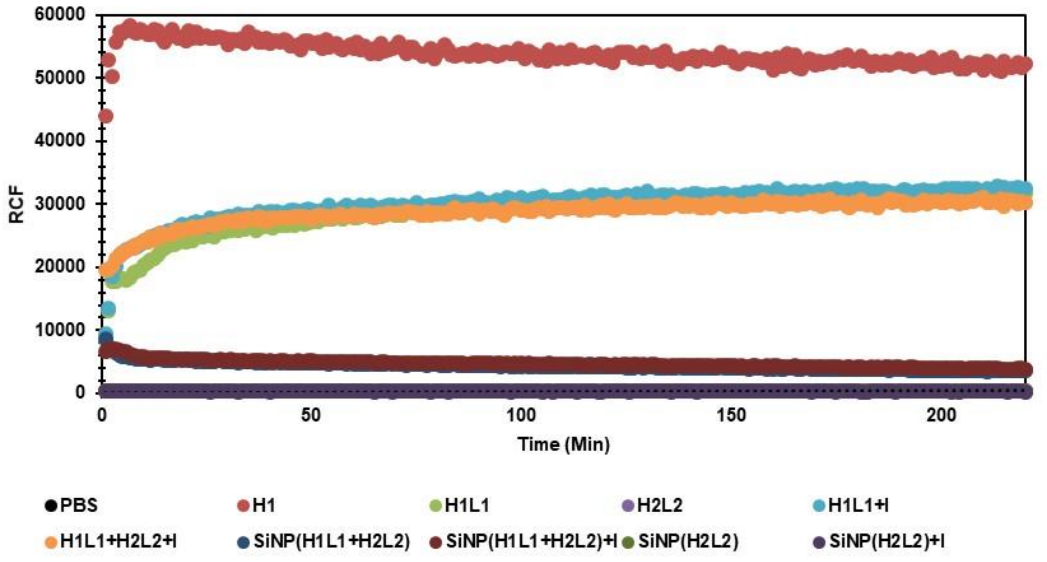

Figure B.2. Time-dependent fluorescence of the hybridization chain reaction on SiNPs.

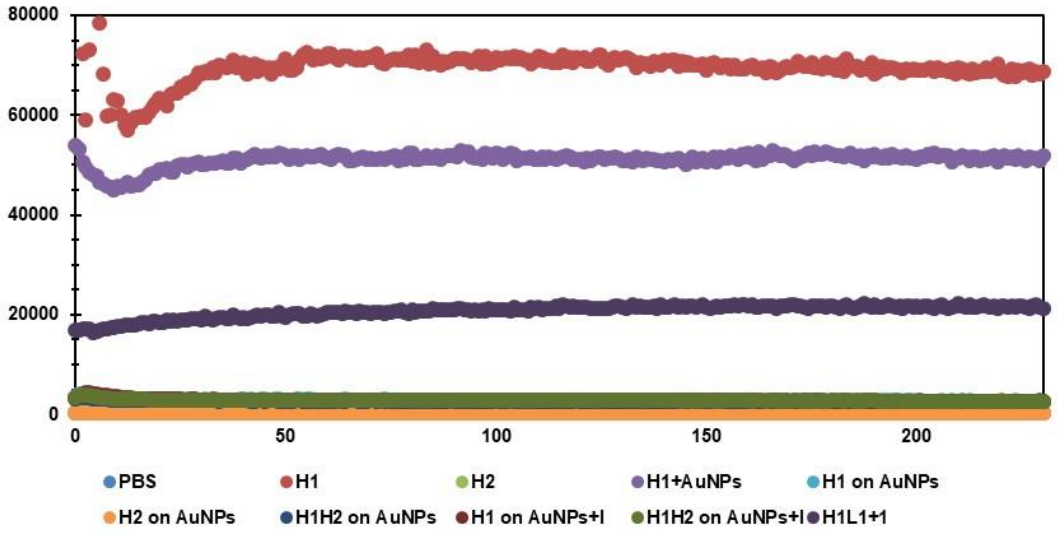

Figure B.3. Time-dependent fluorescence of the hybridization chain reaction on AuNPs.